ACTINIDE RESEARCH QUARTERLY

Ac Th Pa U Np Pu Am Cm Bk Cf Es Fm Md No Lr

First Quarter 2021

Nuclear Thermal Rocket Reactors

A Retrospective 1955–73

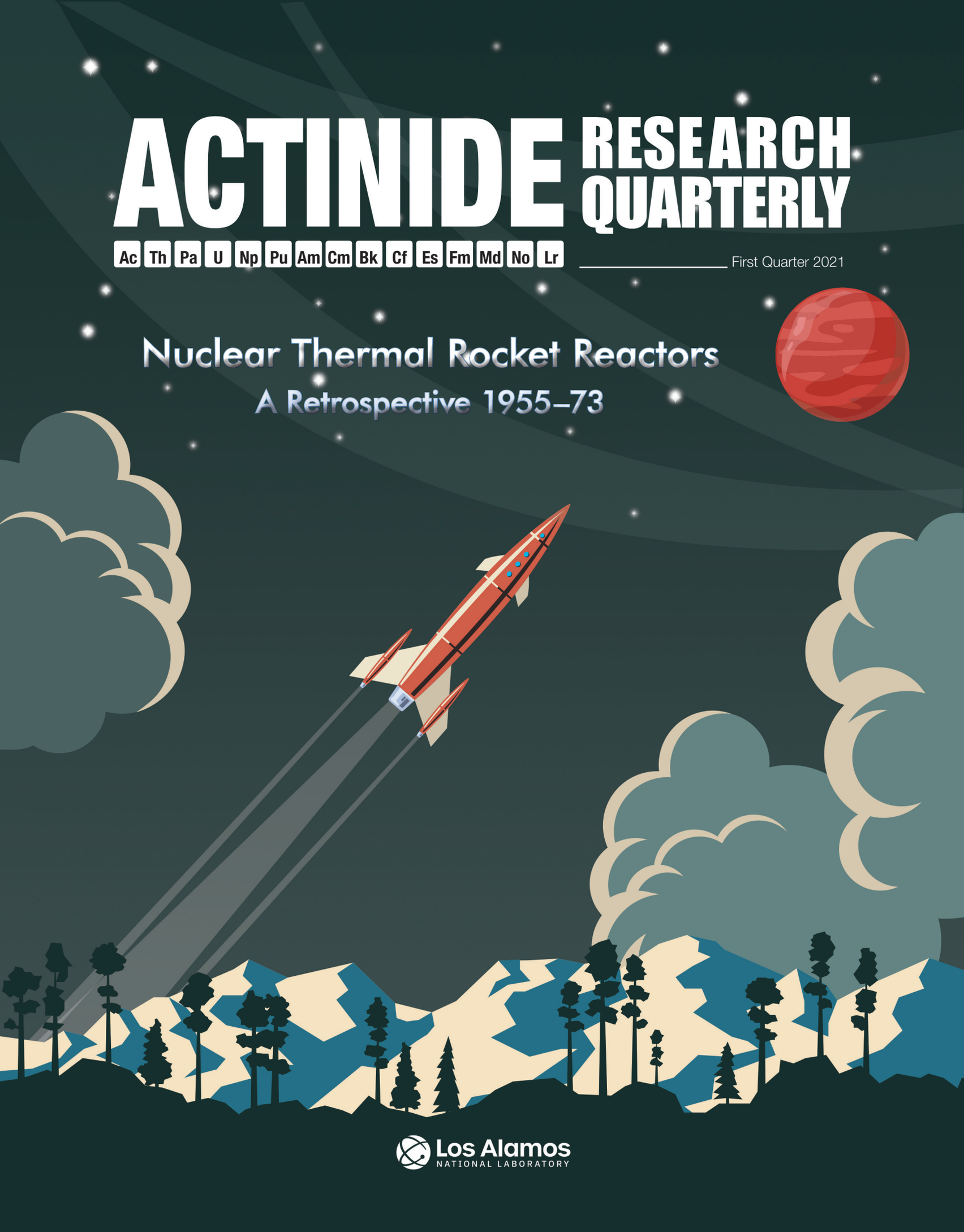

Los Alamos NATIONAL LABORATORY

Foreword

In this issue we are proud to feature articles from a variety of Seaborg-funded Fellows at Los Alamos National Laboratory (LANL), including research from five recent Seaborg postdocs.

Our special cover article has been contributed by Richard Malenfant, a retired Laboratory scientist. In "Nuclear Thermal Rocket Reactors and Engine Systems: A Retrospective," Malenfant details some of the technical lessons that were learned during the major Rover project that ran from 1955–73. The immense engineering challenge represented by nuclear-powered rockets, and their reactor engines, is particularly timely as the nation prepares for a twenty-first century human mission to Mars.

More terrestrial concerns are addressed by Jason Baker, who explains new approaches to the challenges of analyzing nuclear fuels at high pressures (*p14*). In particular, a class of uranium-silicon accident-tolerant fuels are examined.

Two articles cover tricky challenges in condensed matter physics—Laurel Winter explains her work exploring the "hidden order" state in the actinide alloy uranium ruthenium silicide (*p20*). Nicholas Sirica meanwhile describes the curious properties of so-called topological materials, which evade classification using classical definitions, and his search for these phases in the actinide and lanthanide elements (*p33*).

Instrumentation and measurement methods are fundamental to all areas of science, actinides included. We print here research accounts from recent Seaborg Fellows who have been attempting to streamline and improve the fidelity of these methods. On *p26*, Noah Jemison describes a rapid alternative to the standard method for measuring isotope ratios in nuclear materials. Finally, David Frazer outlines a system for reducing sample size for mechanical testing of actinides. This promises to reduce time and cost to current analytic methods as well as provide insight and accelerate nuclear materials development.

Owen Summerscales
Editor

About the cover: Between 1955 and 1973, Los Alamos Scientific Laboratory operated a pioneering program designing and building nuclear thermal rocket reactors for space exploration. We present a technical retrospective here, highlighting some of the engineering lessons learned from this work.

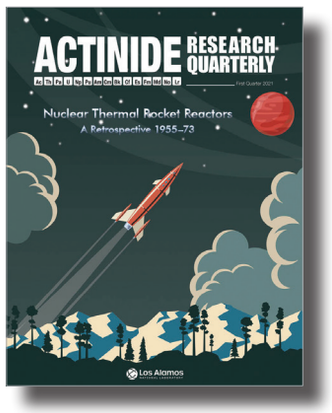

Contents

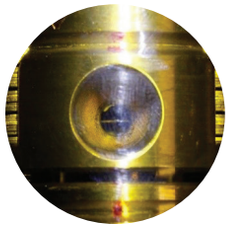

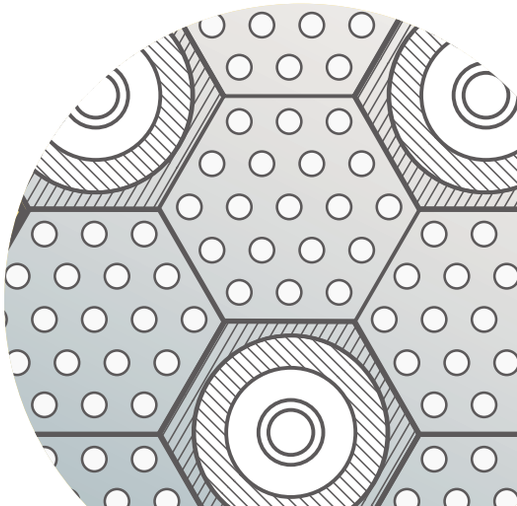

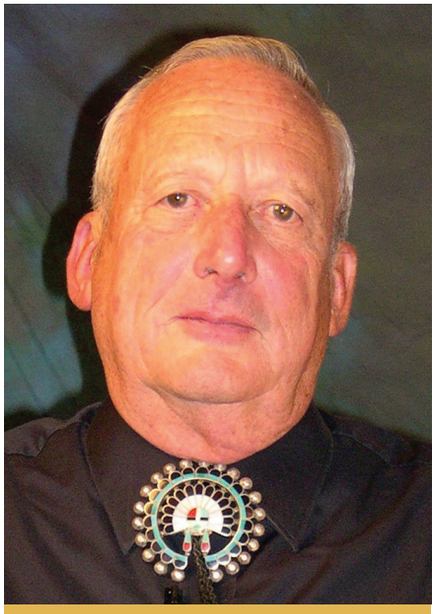

Richard Malenfant

Richard (Dick) Malenfant joined the Critical Experiments Laboratory at the Oak Ridge National Laboratory in 1956. He was called to active duty in the Air Force in 1957 and spent his 3-year tour of duty as a Nuclear Research Officer in the Propulsion Laboratory at Wright Patterson Air Force Base in Dayton, Ohio where he was associated with the theoretical and experimental aspects of nuclear propulsion programs for aircraft, ramjets, and rockets. In January, 1961 he joined the Critical Experiments Laboratory (Pajarito Site) at the Los Alamos Scientific Laboratory. He worked on the Rover nuclear rocket propulsion program until it was cancelled in 1969. Until retirement in 1996, he continued to work on programs of nuclear criticality safety and radiation protection. After retirement, he continued work on nuclear programs including criticality safety and medical isotopes. He maintains an active interest in the history of the work done at the Pajarito Site where he spent most of his time at the laboratory.

Nuclear Thermal Rocket Reactors and Engine Systems: A Retrospective

Richard E. Malenfant,[1] Frank P. Durham,[1] Milton Klein[2]

[1] *Formerly Los Alamos National Laboratory, Los Alamos, New Mexico*
[2] *Formerly NASA/AEC Space Nuclear Systems Office*

From the late 1950s to the early 1970s a major US program successfully developed the capability to conduct space exploration using the advanced technology of nuclear rocket propulsion. The program had two primary elements: Rover and NERVA (Nuclear Engine for Rocket Vehicle Application). Part of the NASA space program, the former provided the basic reactor design, fuel materials development, and reactor testing capability with pioneering work performed by Los Alamos National Laboratory (LANL) and its contractors. NERVA meanwhile was focused on engine development by the industrial team of Aerojet and Westinghouse, building on and extending the Los Alamos efforts for flight system development. The challenge of this part of the program was designing nuclear engines that could survive the shock and vibration of a space launch.

Together, these programs demonstrated the space-practical operation capabilities of nuclear thermal rockets, which would be launched from Earth orbit, and established a technology base that includes proven nuclear thermal rocket capabilities, including:

(1) Over double the specific impulse of chemical propulsion systems (and nearly triple that of chemical rockets with the same exhaust gas temperature).

(2) Thrust capabilities in the range 10,000–250,000 pounds of thrust.

(3) Practical thrust-to-weight ratios for future NASA space exploration missions, both manned payloads to Mars and unmanned payloads to the outer planets. The objective of a mission to Mars was announced out in 1969, and scheduled for 1981.

This article summarizes the lessons learned in the development of this technology, illustrating that surprises are certain to be encountered when undertaking such advanced programs. Because of the speed with which the program was conducted, many—if not most—of the experimental results were reported only in informal progress reports. The program began under the military during the Cold War, resulting in classification of this material until program termination. At that time, data were declassified wholesale, much of which were subsequently destroyed.

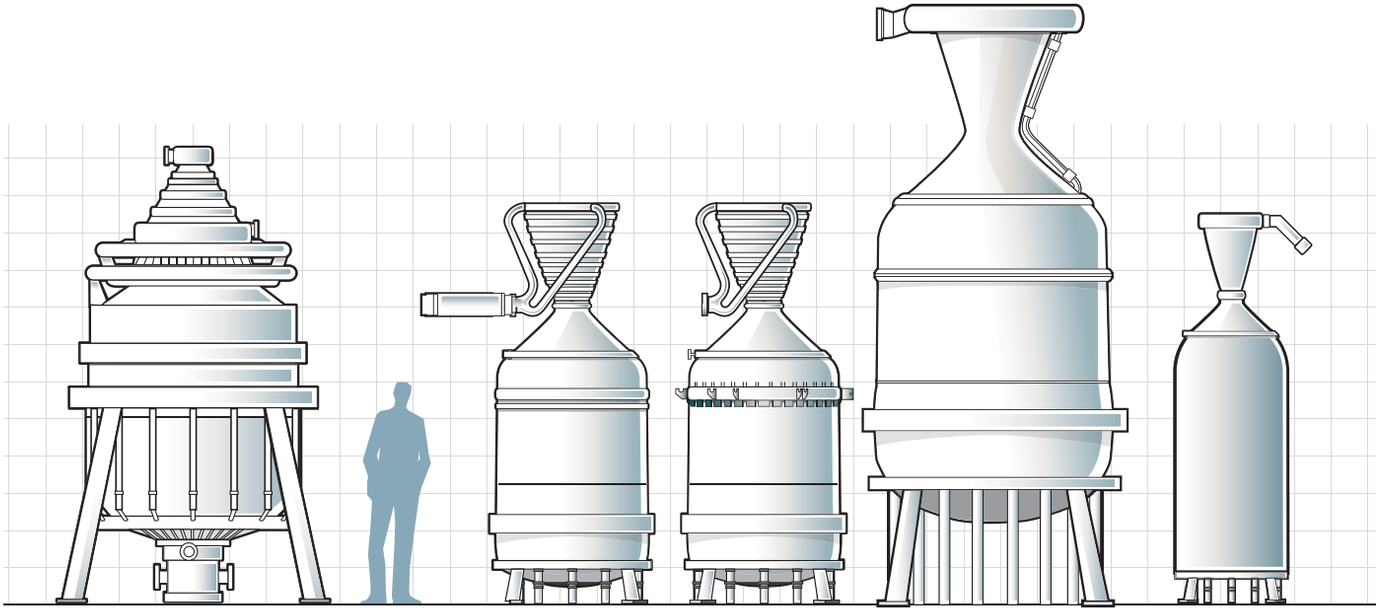

Kiwi-A	**Kiwi-B**	**Kiwi-B**	**Phoebus 2**	**Peewee**
1958–60	1961–64	1965–66	1967	1967
100 MW	1,000 MW	1,000–1,500 MW	5,000 MW	5,000 MW
0 lbs thrust	50,000 lbs thrust	50,000 lbs thrust	250,000 lbs thrust	250,000 lbs thrust

Comparison of Rover nuclear rocket reactors.

Those who cannot remember the past are condemned to repeat it.

The Life of Reason [1905-1906],
Vol. I, Reason in Common Sense
George Santayana

This quotation is particularly appropriate for the lessons learned during the nearly 20 years of the research, development, and demonstration of the Rover and NERVA programs. Surprisingly, designing a reactor to achieve criticality was the least of the problems. Innovative work had to be performed to store and pump liquid hydrogen, and to develop materials capable of withstanding the harsh environments both inside of the reactor core and external to the rocket engine. The radiation heating in the core and the surrounding structure had to be considered as well as the environment external to the engine. Everything inside of the core and surrounding structure had to be cooled, and heating was inconsistent during operation. Finally, the exhaust (or propellant) gas temperature needed to be maximized.

The technical aspects to these extreme conditions included flowing liquid hydrogen, a reactor startup with the high positive coefficient of reactivity for hydrogen changing phase from liquid to high temperature gas during transit through a four foot long core, radiation heating capable of melting tungsten (a sample of insulated tungsten outside of the pressure vessel was melted during the Kiwi B4E test in August, 1964), and temperature gradients of thousands of degrees per millimeter (the main difference between reactors used for rockets and those for electricity is that the temperature must be maximized in rockets). These are just a sampling of the unknowns that were to be addressed. Radiation levels were measured in orders of magnitude such as 10^5.

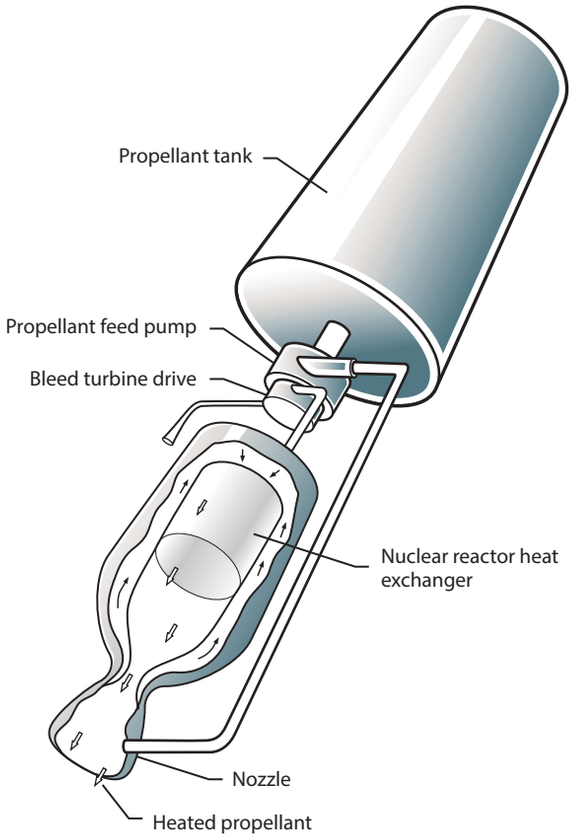

Schematic of a nuclear rocket propulsion motor.

Justification of nuclear power for rockets

The results of numerous studies over the past 50 years have described the advantages of nuclear heat exchanger rocket engines. The bottom line—high thrust and specific impulse (Isp). Although there are systems such as ion propulsion that have higher specific impulse, and other systems that offer higher thrust, there is nothing that provides the unique combination of relatively high thrust and high specific impulse. Specific impulse may be thought of as propulsion efficiency. Measured in seconds, it is approximated as the ratio of thrust measured in pounds divided by the flow rate expressed in pounds of propellant per second. Specific impulse may be expressed as the square root of the absolute temperature divided by the molecular weight of the of the exhaust gas. At the same exhaust gas temperature—usually limited by material considerations of the nozzle—a nuclear heat exchanger rocket using hydrogen as the propellant is nearly three times as efficient as a chemical rocket because of the propellant's lower molecular weight. For missions originating in Earth orbit, the initial weight in orbit varies inversely as the specific impulse. It is not considered necessary to elaborate beyond these basic facts.

Reactor testing

Lessons were learned from every single experiment, and those lessons were then factored into subsequent experiments. Following the Kiwi-A series experiments in 1959–60 with five to six minute bursts operating at outputs from 70–100 MW, an ambitious experimental program was laid out to achieve a 5,000 MW test with Phoebus 2A before the end of the 1960s (N.B., Kiwi refers to the flightless bird, indicating the experimental nature of these reactors which were not designed for

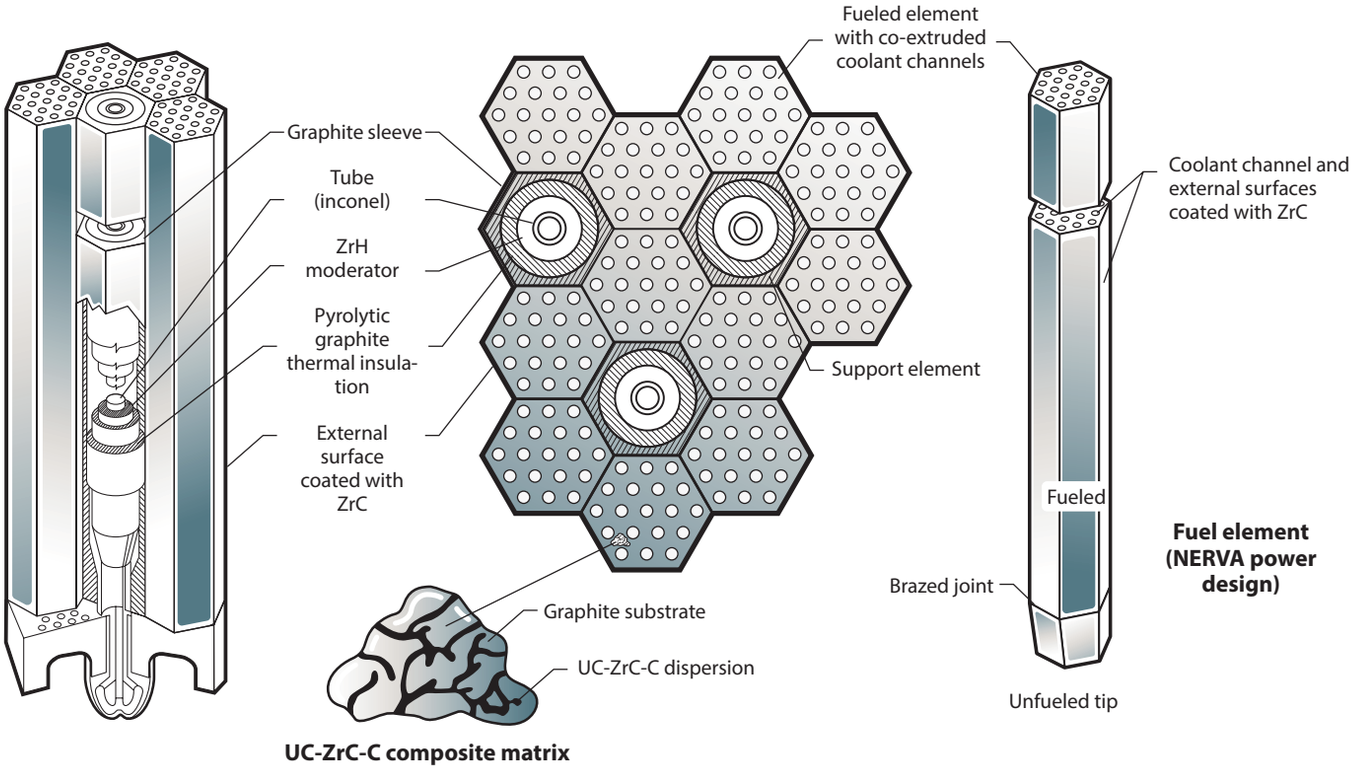

Above: Fuel element (right) and support-element (left) details for Rover and NERVA nuclear rocket reactor cores. The fuel was a composite which consisted of a uranium carbide-zirconium carbide dispersion in the graphite substrate.

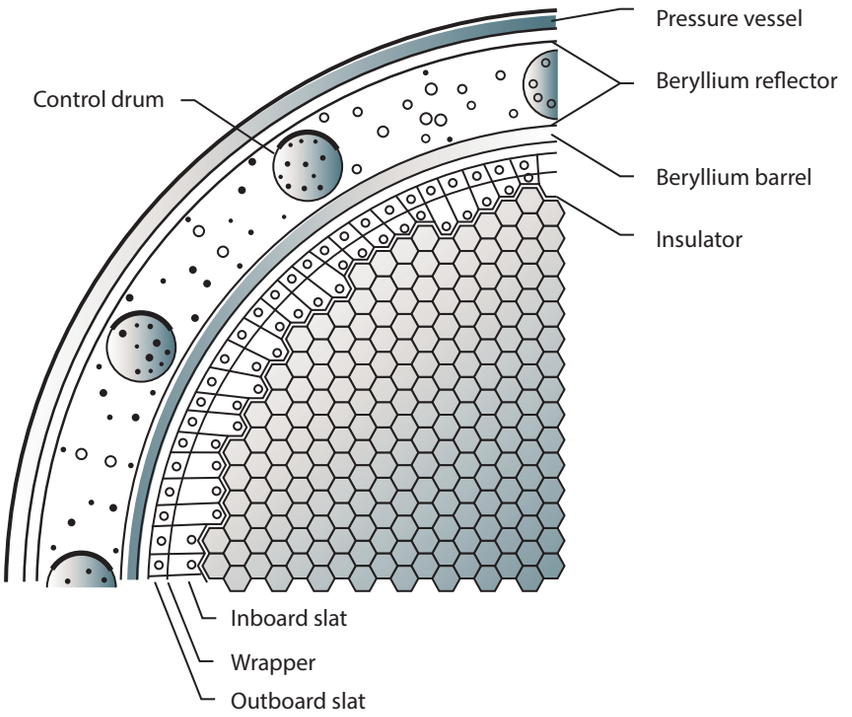

Cross-sectional schematic of a Rover nuclear rocket reactor.

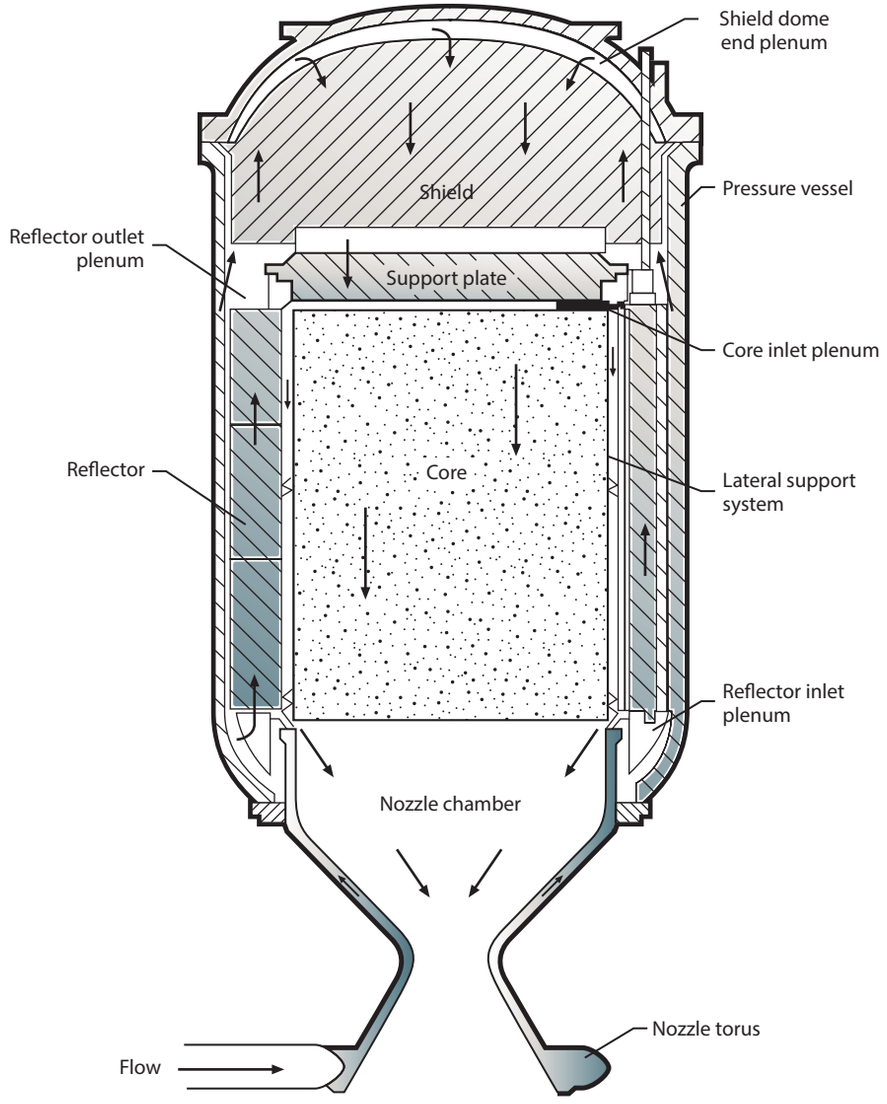

Reactor propellant-flow schematic for a nuclear rocket propulsion motor.

• • •

flight; Phoebus is often used as a poetic name for the Sun, from ancient Greek). The development of Phoebus 2A resulted in the most powerful nuclear propulsion reactor ever built.

In addition to the Kiwi Transient Nuclear Test in January, 1965, 12 experiments were conducted prior to Phoebus 2A. These included three full engine tests at 1,100 MW for 60 minutes in a single run designated NRX-A3, NRX-EST, NRX-A-5, and NRX-A6 (April, 1965; February–March, 1966; June, 1966; December, 1967). Additional experiments were conducted with Peewee including PW-1 (the Peewee reactors were small test-beds that operated at full power density to aid in fuels development; December, 1968). The first down-firing prototype nuclear rocket engine, XE, was operated for a total of 115 minutes of powered operation with 28 restarts. This was the last NERVA test due to the termination of the program.

Innovations in the program

In this section, a few examples of innovations, challenges, unusual experiments, and technology developments resulting from the Nuclear Rocket Program are listed below to serve as examples.

Reactor power is usually measured by observing the magnitude of neutron leakage once calibrated with flow rate and temperature increase. To measure this power in a nuclear rocket engine prototype, two major problems had to be addressed. First, radial power density (fission rate) is affected by the position of the control vanes. Control of the reactors meanwhile was implemented by rotary control vanes in the beryllium reflector. Boral vanes covered 120° of the cylindrical control "rods" (Boral is a mixture of boron, usually as the carbide, in an aluminum matrix). Neutron leakage, and hence the inference of reactor power, is a function of control vane angular position. A second complication was measuring exit gas temperature. Standard thermocouples consist of a pair of dissimilar wires terminating in a small metal tip. The high-temperature couples were typically composed of tungsten/tungsten-rhenium sheathed in a high-temperature metal. Specific heating from radiation is greater in the metal of the thermocouple than in the gas, therefore the unfortunate possibility was that we were measuring the temperature of the thermocouple rather than that of the gas. This was overcome by the development of specialized thermocouples to measure the exit gas temperature.

Another problem was the unwanted formation of methane from hot hydrogen gas reacting with graphite in the fuel at the exit end of the core. This was addressed by cladding the fuel elements with niobium or zirconium as part of a lengthy program of materials development.

The flow of hydrogen through the core places the fuel elements in tension—and the graphite elements have little strength in tension. To address this problem, the fuel elements were held in compression by a metal tube running the full length of the fuel element. However, that metal tube had to be cooled. If the hydrogen gas that cooled the "tie tube" were exhausted directly into the nozzle, the specific impulse would suffer because gas through the tie tubes was cooler than that through the core. This was addressed by a double pass through the tie tube back up into the inlet plenum so that all of the gas exiting into the exhaust plenum had passed through the core proper.

One of the more interesting problems, although also tedious at times, was flattening the power density distribution and tailoring the flow to each individual channel in the fuel. The power density was flattened by varying the uranium density in the fuel. In addition, each and every hole in the fuel elements was orificed to tailor the cooling to the power extracted from that hole. There were 19 holes in most elements, and about 1,500 elements in each Kiwi, Phoebus 1, or NRX reactors. This required determination of the power for every single one of the nearly 30,000 holes and the tailoring of the flow to optimize exhaust gas temperature.

After evaluating mission reliability, we considered clustering the nuclear rocket engines. This led to a unique experiment in which two nearly identical Rover reactors were operated side-by-side to evaluate the neutronic coupling. Since the degree of interaction was quite small, the fission rate in one of the reactors was oscillated by rotating a control rod to allow a measurement of the transfer function. In addition to evaluating the neutronic coupling, this measurement allowed us to verify the time necessary for fission distribution in a nuclear reactor to achieve normal mode when excited by an asymmetric external source.

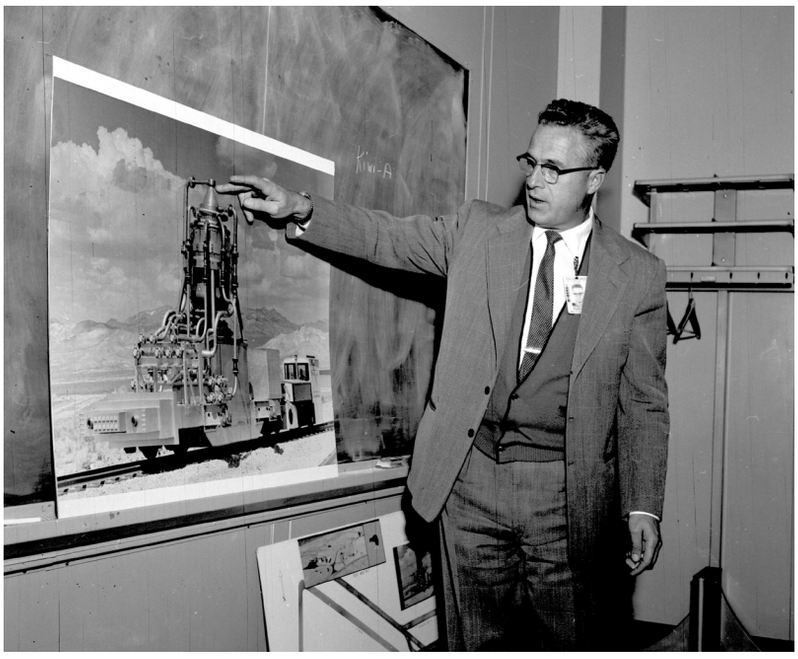

Raemer Schreiber with a Project Rover poster, January 1959.

• • •

In order to protect the structure of the test cell from radiation heating, all tests following Phoebus 1A were performed inside of a well shield. The shield consisted of an aluminum shell cooled with boron-loaded water. The effect of the shield on reactivity was carefully measured. During the test of the 4,000 MW Phoebus 1A, 60 MW was absorbed by the shield due to a combination of radiation heating and n,α reactions in the boron. The boron was necessary to reduce the more penetrating gamma radiation that would otherwise result from the 2.23 MeV gamma-rays from neutron capture in hydrogen (neutron capture in boron also results in a less-penetrating 0.51 MeV gamma-ray). The boron was not really necessary to reduce neutron backscattering from the shield.

The next generation

In 1983, the Strategic Defense Initiative ("Star Wars") identified missions that could benefit from rockets more powerful than chemical rockets, and in the same year a nuclear propulsion project, SP-100, was created with the aim of developing a 100 kW nuclear rocket system. This became a secret project codenamed Project Timber Wind from 1987 to 1991 that was later expanded into the Space Nuclear Thermal Propulsion (SNTP) program at the Air Force Phillips Laboratory (Albuquerque, NM). This ran until 1994 as NASA deemed it had no significant improvement over the Project Rover design.

In 2013, engines were examined at the Marshall Space Flight Center (Huntsville, AL) for Earth to Mars interplanetary travel, with a focus on nuclear thermal rocket engines. The shorter flight duration would reduce crew exposure to potentially harmful cosmic rays and reduce the impact on the human body of exposure to micro-gravity. The difference in flight time was estimated at four versus nine months using nuclear and chemical engines, respectively. The Mars Design Reference Architecture selected engines of the type developed in Project Rover and in 2019, Congress approved $125 million in funding for the development of nuclear rockets.

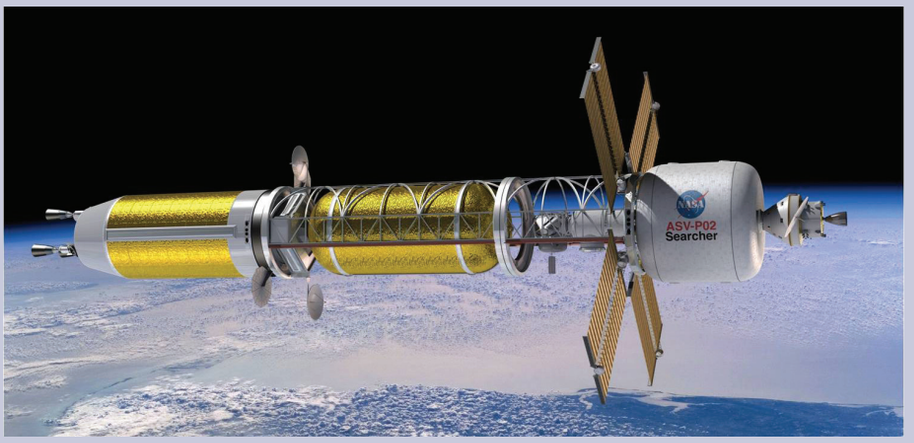

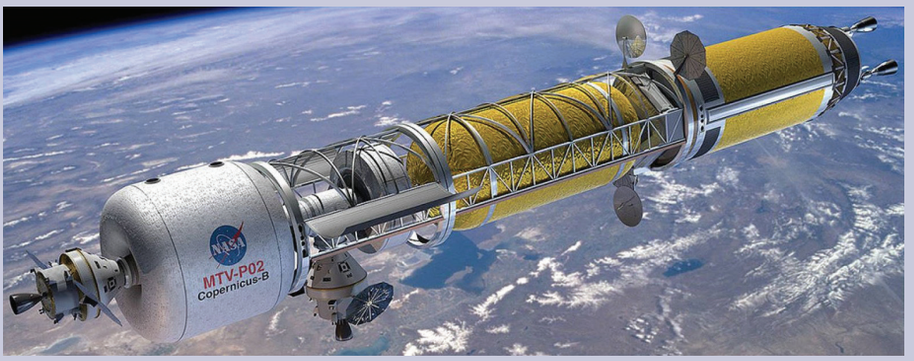

NASA rendition of a nuclear thermal propulsion enabled spacecraft mission, outward bound. Credits: NASA.

Twenty-First Century Human Mission to Mars

In 2010, Barack Obama promoted the idea of a crewed mission to orbit Mars by the mid-2030s, followed by a landing. This was supported by Donald Trump in 2017 who signed a directive with private sector partners for a human return to the Moon by 2024, followed by missions to Mars and beyond.

Nuclear thermal propulsion remains an attractive technology to propel human exploration missions to Mars and other deep space destinations. Furthermore, recent advances in materials technology may provide a more affordable pathway to development of a nuclear rocket engine. In the Rover/NERVA programs, highly-enriched uranium was chosen as the fuel, whereas now, low-enriched uranium is being examined as an alternative. This could save money, reduce security issues, and potentially be less impactful on test site locations. The other key area is to examine a new ceramic-metallic fuel form which eliminates erosion and cracking, which the original graphite composite rods suffer from.

The legacy of the Rover/NERVA programs

The legacy of the nuclear thermal rocket program must not be lost. Environmental, safety, and health considerations were carefully considered during all experiments in the nuclear rocket program. However, it is likely that the experiments essential to the development of the NERVA program could not be repeated in the United States today short of a national emergency. Therefore there is a strong need to recover, to the extent possible, the legacy of the Rover/NERVA programs. To assist in this effort a short list of references is included.

The significant advantage of relatively high thrust and specific impulse will likely result in the use of nuclear power for ambitious space missions in the future. The legacy of the Rover/NERVA programs provides the United States with a wealth of data. However, the major lesson learned from the program was to expect the unexpected. Continued experiments are essential to extend the information obtained in the fifteen years of the active program. The Rover/NERVA program was conducted during the Cold War. The military birth of the program resulted in classification and restricted distribution of material until program termination. At that time, data were declassified wholesale—"Rover Declassified" was stamped on hundreds of documents, many of which were destroyed. Perhaps the memories of those who were fortunate to be part of the program can be mined before the experience is lost forever.

Further reading:

1. *G.L. Bennett, et al., "Prelude to the future: A brief history of nuclear thermal propulsion in the United States," in "A critical review of space nuclear power and propulsion," 1984–1993, edited by M. El-Genk, New York: American Institute of Physics Press, 1994, 221–267.*
2. *R.J. Bohl, et al., "Nuclear rocket review," LANL document LA-UR-91-20-20, 1991.*
3. *R.W. Bussard, R.D. DeLauer, "Nuclear rocket propulsion," McGraw-Hill Book Co., Inc., 1958.*
4. *J.A. Dewar, "Project Rover: A study of the nuclear rocket development program, 1953–1963," US Department of Energy, Washington, DC, 1974.*
5. *S.V. Gunn, "Development of nuclear rocket engine technology," AIAA paper 89–2386 presented at AIAA/ASME/SAE/ASEE 25th Joint Propulsion Conference, Monterey, CA, 1989.*
6. *D.R. Koenig, "Experience gained from the space nuclear rocket program (Rover)," LANL report LA-10062-H, 1986.*
7. *J.M. Taub, "A review of fuel element development for nuclear rocket engines," Los Alamos Scientific Laboratory report LA-5931, 1975.*
8. *C.W. Watson, "Nuclear rockets: High-performance propulsion for Mars," LANL report LA-12784-MS, 1994.*

Project Rover Archival Photos

Raemer Schreiber headed LASL's Rover program as Nuclear Rocket Propulsion (N) Division leader in 1955. In 1962, he became Technical Associate Director, with responsibility for the entire nuclear rocket propulsion program.

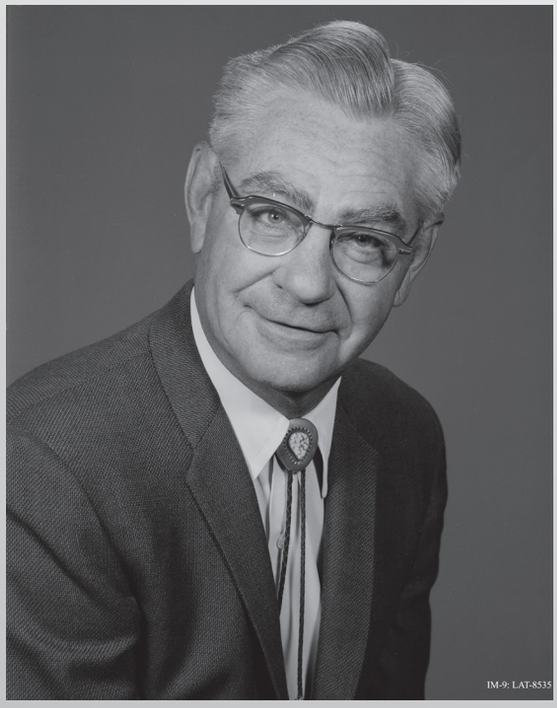

Roderick Spence took over as N Division leader after Schreiber in 1958.

Henderson, McCord, Holloway, Schreiber, Warner.

Taschek, Richard, Raemer Schreiber, Perkins, Duncan MacDougall, and Harold Agnew 1974.

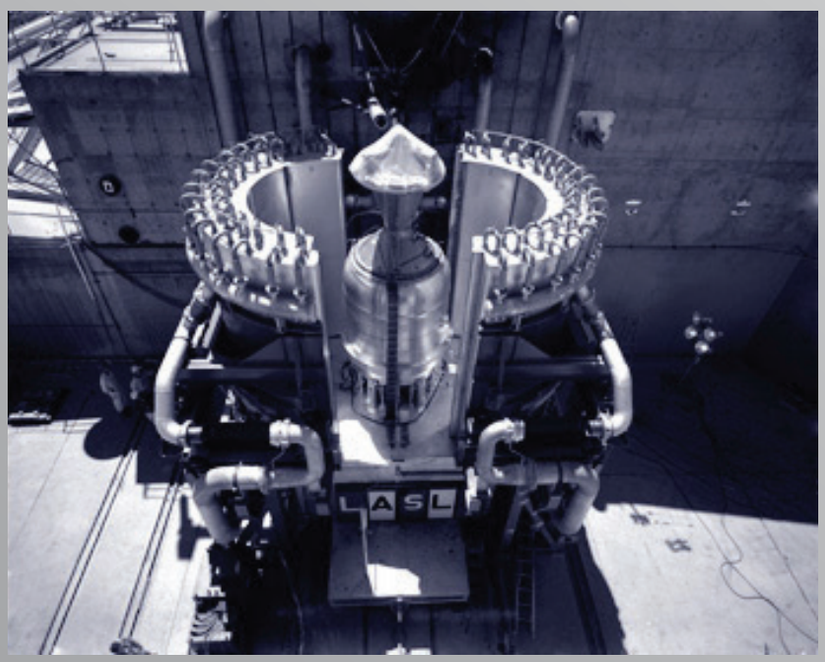

The Phoebus-2A being prepared for testing at Los Alamos Scientific Laboratory (LASL). Photo courtesy of Richard Malenfant.

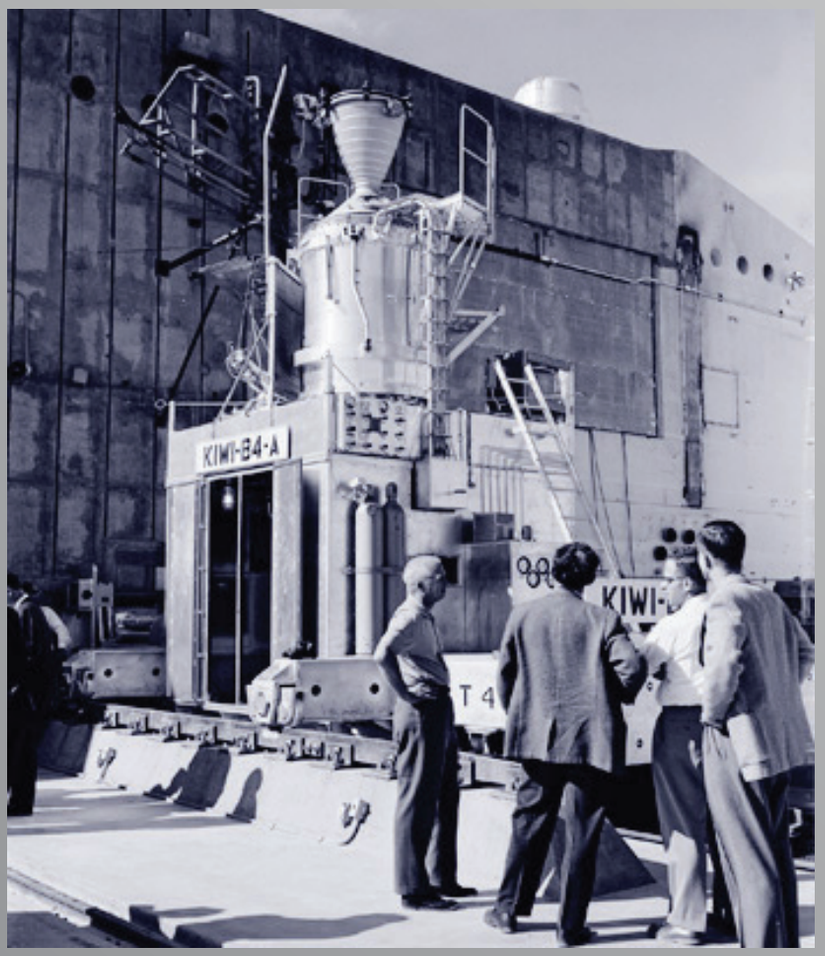

The Kiwi-B4A reactor awaits testing at the Nevada Test Site in 1962. At the left is Norris Bradbury, Laboratory Director from 1940–970.

Robert Hanrahan stands between the Kiwi-A (*left*) and Phoebus-1 (*right*). Phoebus-1 is now at the Atomic Testing Museum in Las Vegas, Nevada. Archival photo courtesy of Robert Hanrahan.

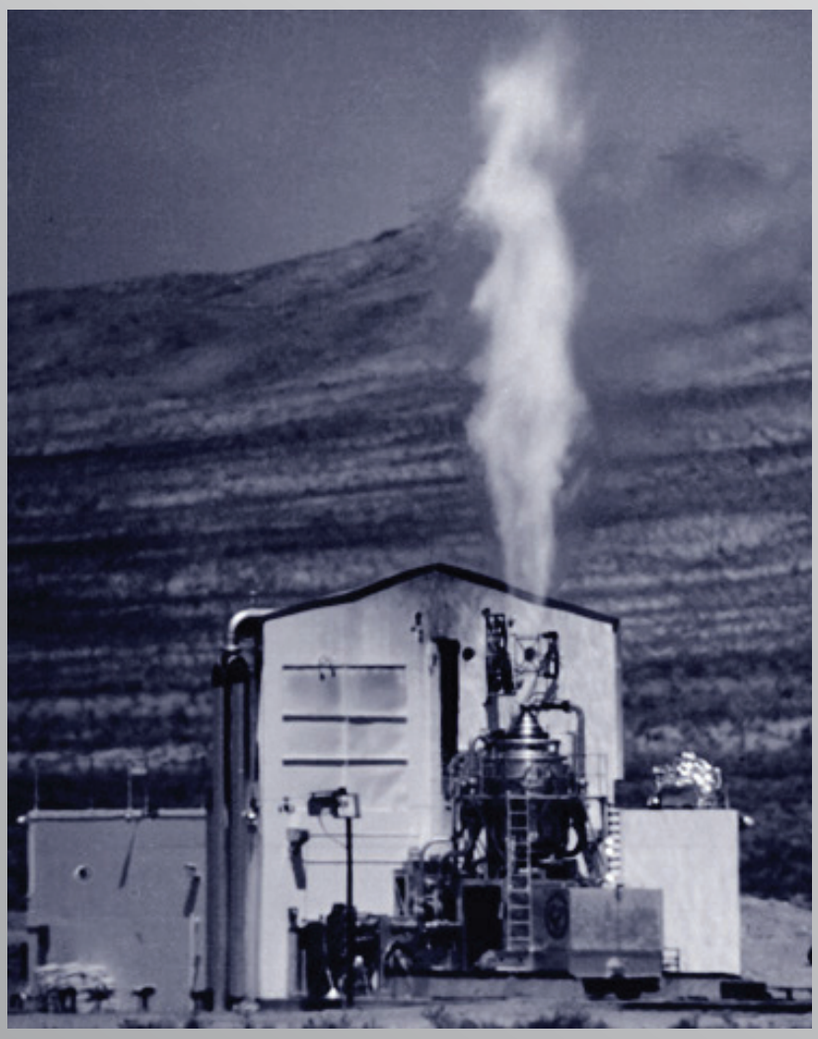

Proof of principle was demonstrated with the 100 MW Kiwi-A. Three versions of Kiwi-A were operated at Test Cell A, Nevada Test Site 1956–1960.

Jason Baker

Jason Baker was a Seaborg Fellow under the mentorship of Hongwu Xu and Andrew Gaunt from 2018 to 2020 in Earth Systems Observations (EES-14). His research was focused on understanding the high-pressure behavior of nuclear-fuel materials. He is now a Research Scientist in the Materials Dynamics and Kinetics group (MDK) at Lawrence Livermore National Laboratory in Livermore, California.

Exploring Nuclear Fuels at High Pressure and Temperature: From Cradle to Grave

Jason Baker
Lawrence Livermore National Laboratory, 7000 East Ave, Livermore, California

Actinide materials are of great importance due to their wide-ranging uses in modern industry. For example, uranium dioxide (UO_2) is used as the primary nuclear fuel in light-water reactors (LWRs). However, nuclear reactor accidents such as the Fukushima disaster in 2011 have encouraged the nuclear energy industry to explore alternative accident-tolerant nuclear fuels (ATNFs) such as uranium-silicide (U-Si) compounds. A number of U-Si phases (e.g., U_3Si_2, U_3Si_5) possess higher thermal conductivities than the conventional UO_2 fuel under nuclear reactor operating conditions. Higher thermal conductivities allow better heat dissipation in ATNFs when used in reactors. Nonetheless, significant research is needed to understand their structural stability and physical properties (e.g., mechanical properties) under both ambient conditions and those of elevated pressures and temperatures. An important elastic property significant to ATNF mechanical integrity is compressibility (i.e., inverse of bulk modulus). A powerful tool to study mechanical properties is applied pressure due to its ability to change structural characteristics. By applying pressure in concert with X-ray diffraction (XRD) technique, structural behavior and mechanical strength can be examined.

At the end of the nuclear fuel cycle, storage of used fuel and high-level waste becomes a significant concern. It is imperative to understand actinide-water interactions due to the potential of these wastes to react with underground water during long-term storage in geological repositories. This is especially true under hydrothermal conditions induced by the decay heat from radioactive wastes while stored in the subsurface repositories. In these aqueous environments, uranium frequently occurs as an aqueous ion, like uranyl (UO_2^{2+}), which has a tendency to interact with ligands (e.g., chloride, carbonate) present in groundwater. High pressure and temperature (P/T) conditions can also significantly change the properties of water, such as decreasing its dielectric constant with increasing temperature. These changes may subsequently result in significantly different chemistries at hydrothermal conditions. In order to probe changes in aqueous actinide species as a function of pressure and temperature, we can use the effective combination of X-ray absorption spectroscopy (XAS) coupled with hydrothermal cells.

Diamond anvil cells to produce high pressures and temperatures

Diamond anvil cells (DACs) are devices capable of producing pressures expected at the center of planets (> 100 GPa). They achieve these incredible pressures by exploiting the grade-school physics equation P = F/A (where P is pressure, F is force, and A is area). Large pressures are achieved by applying a force to an extremely small area (samples are typically a few micrometers in size). Diamonds have a large swath of scientific applications and properties outside of their typical consumer

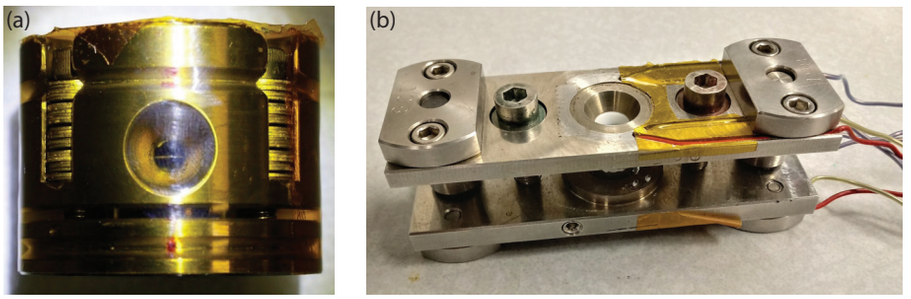

Figure 1. (a) Princeton symmetric type diamond anvil cell. (b) Two-post hydrothermal diamond anvil cell.

• • •

attributes, such as the hardest of known materials, and transparency to a wide range of the electromagnetic spectrum. Furthermore, combined with resistive heating and laser heating techniques, DACs are capable of producing high pressure and temperature simultaneously, enabling access to a large range of P/T conditions.

For our studies, two different types of DACs were used. For XRD measurements of U-Si compounds, a Princeton-type symmetric DAC was utilized (Fig. 1a). Force is applied through tightening of the screws shown in the photograph. For our particular study of U_3Si_5, pressures up to 16.7 GPa were attained at room temperature. For XAS measurements of aqueous uranium solutions, a hydrothermal DAC was employed (Fig. 1b). It can achieve pressures up to 10 GPa. Simultaneously, high temperatures (up to 1200 °C) can be achieved through a resistive coil heater attached to each side of the DAC near the diamond crystal. The pressure and temperature ranges of particular interest for our study of aqueous U(VI) species are up to 500 MPa and 200 °C, respectively.

High-pressure X-ray diffraction of U_3Si_5

High pressure X-ray diffraction is a scattering technique that allows for determination of crystal structures of materials as a function of pressure. We performed synchrotron XRD measurements on U_3Si_5 from 2.6 to 16.7 GPa at the Advanced Photon Source, Argonne National Laboratory (Fig. 2a) in order to determine whether U_3Si_5 undergoes any pressure-induced phase transition and its mechanical properties such as bulk modulus. The unit-cell parameters (*a*, *b*, and *c*, corresponding to the three axes of the crystal structure) of U_3Si_5 were derived from the obtained XRD data by whole-pattern LeBail analysis.

The ambient crystal structure of U_3Si_5 is of hexagonal type (Fig. 2b inset). This structure remains stable up to 16.7 GPa, the highest pressure tested in our experiments, as evidenced by the lack of change in XRD patterns (Fig. 2a). From these patterns, the unit-cell parameters a (= b) and c were determined (Fig. 2b). The a-axis is found to be less compressible than the c-axis, indicating a significant anisotropy. This difference is attributed to the lack of U–Si bonds along the c-axis (the vertical direction in Fig. 2b inset) compared to the a and b axes.

From unit-cell parameters a and c, unit-cell volume (V) can be calculated for each pressure, which can then be used to determine the bulk modulus (i.e., inverse of compressibility). The data show a steadily decreasing volume with pressure increase (Fig. 2c). From this variation, we fitted an equation of state (EOS) which is parameterized to determine the bulk modulus of a material—for U_3Si_5 the value was

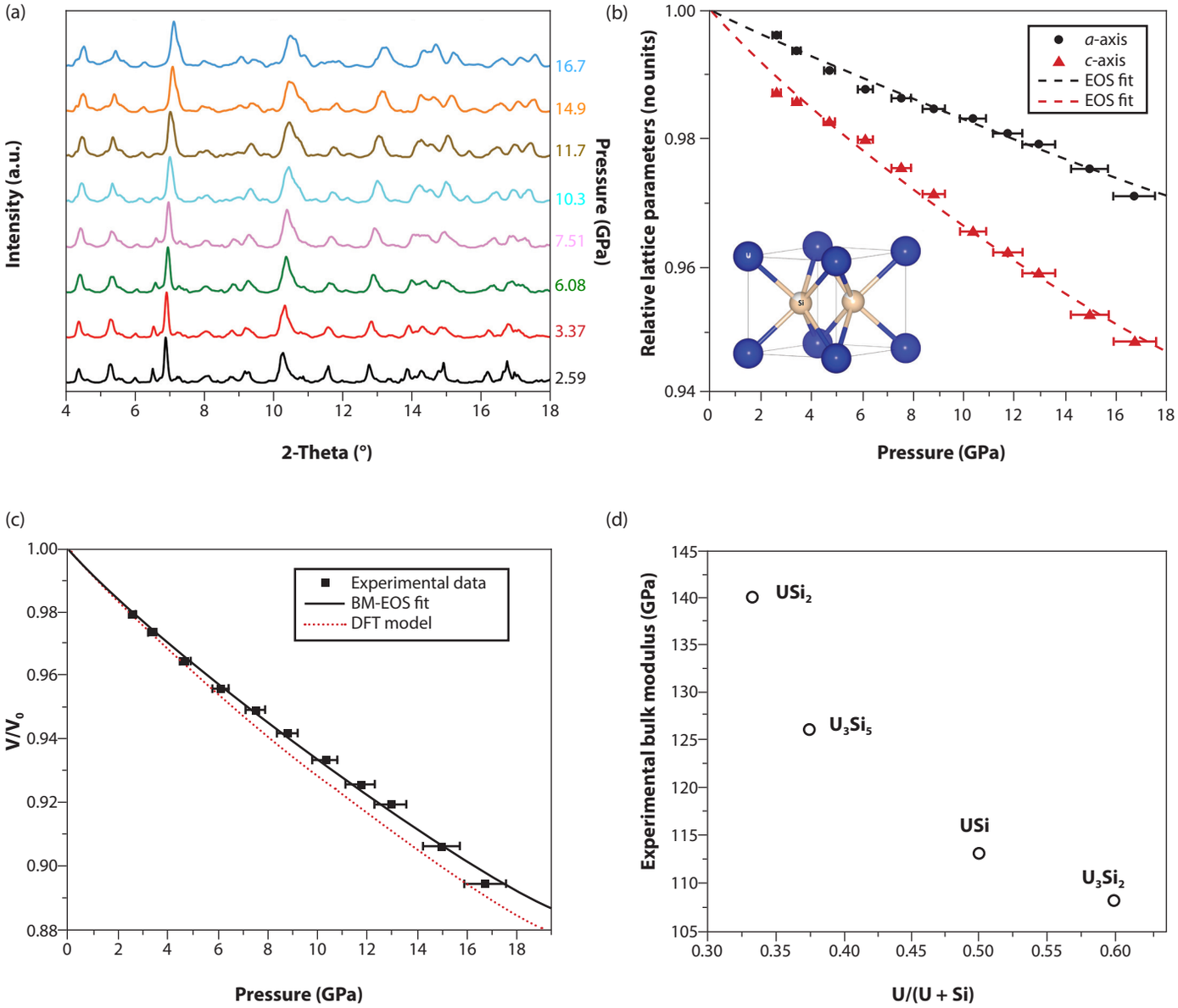

Figure 2. (a) X-ray diffraction patterns at elevated pressures (2.59–16.7 GPa). (b) Unit-cell parameters *a* and *c* of U_3Si_5 as a function of pressure. The *a*-axis is found to be less compressible (more shallow slope) than the *c*-axis (steeper slope), indicating a significant anisotropy. (c) Unit cell volumes of U_3Si_5 as a function of pressure along with an equation of state (EOS) fit (solid line) and the EOS calculated by density functional theory (dotted line). (d) Experimentally determined values of bulk moduli of U-Si compounds as a function of U/U+Si ratio.

determined as 126 GPa. The bulk modulus, in a general sense, gives a measure of how resistant a material is to compression where a larger value means more resistance to compression. If this is compared to other U-Si accident-tolerant nuclear fuels such as USi, U_3Si_2, and USi_2, a trend of decreasing bulk modulus (i.e., increasing compressibility) is observed with increasing U/U+Si ratio (Fig. 2d). Thus, we conclude that increasing uranium content (larger value of U/U+Si) leads to a "softer" or more compressible U-Si compound.

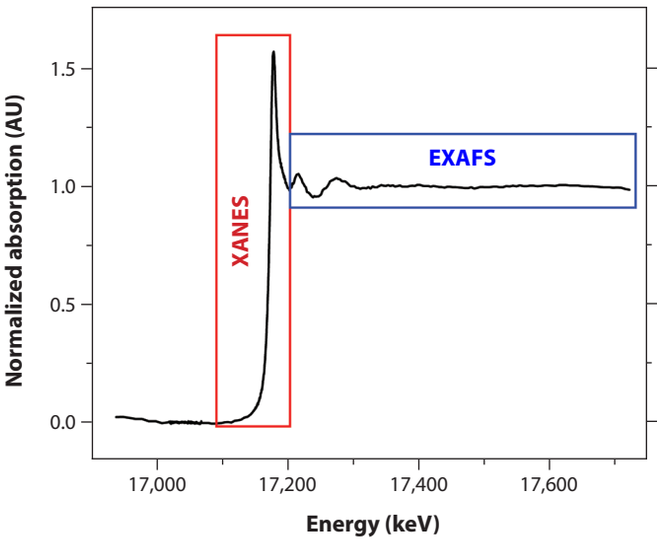

Figure 3. Uranium L_{III}-edge X-ray absorption spectra of $[UO_2(Cl)_n(H_2O)_{5-n}]^{2-n}$ aqueous solution with $[Cl^-] = 6$ M at 25 °C. Boxed regions indicate X-ray absorption near-edge structure (XANES) and extended X-ray absorption fine structure (EXAFS). The XANES region can be used to determine oxidation state and the EXAFS region can be used to determine nearest-neighbor interactions.

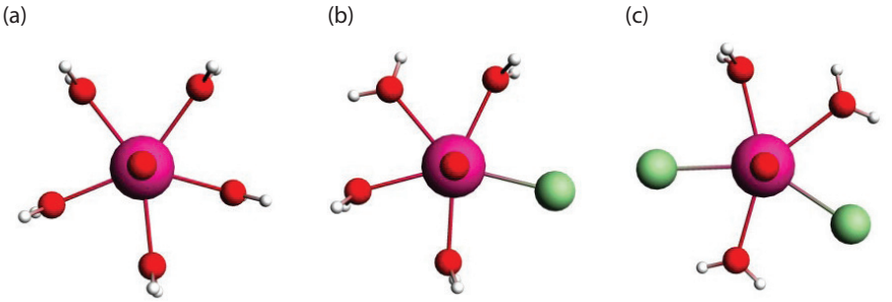

Figure 4. Density functional theory derived structures of $[UO_2(Cl)_n(H_2O)_{5-n}]^{2-n}$ for (a) n = 0, (b) n = 1, and (c) n = 2. These models are used to aid EXAFS data analysis.

X-ray absorption spectra of uranyl under hydrothermal conditions

Synchrotron X-ray absorption spectroscopy is a technique that probes the energy structure near an atom's specified absorption edge to yield information about the molecular structure. An X-ray absorption spectra can be separated into two main regions, near-edge and fine structures (XANES and EXAFS, respectively; Fig. 3). The XANES region provides insight into the oxidation state of the absorber atom; the EXAFS region informs us of nearest neighbor interactions of the absorber atom. Combining both regions and density functional theory (DFT) calculations, we can reliably determine the oxidation state, bond distance, and coordination chemistry. In our experiments, we performed XAS measurements around the U-L_{III} edge (17166.3 eV) at the Stanford Synchrotron Radiation Lightsource (SSRL), SLAC National Accelerator Laboratory, on $[UO_2(Cl)_n(H_2O)_{5-n}]^{2-n}$ aqueous solutions at various chloride concentrations up to 200 °C. We are interested in the chemical coordination of U(VI) with chloride (Cl^-) because Cl^- is among the most common ligands present in groundwater.

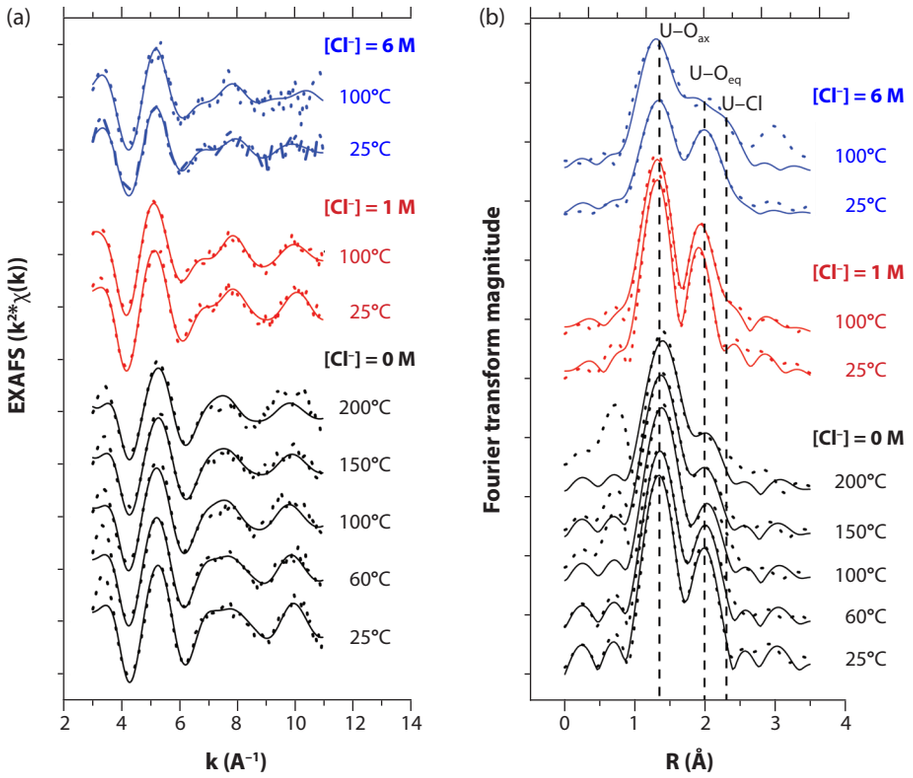

Figure 5. (a) EXAFS spectra for various Cl^- concentrations and selected temperatures. The dotted curves represent the experimental data and the solid curves represent the fits using UO_2^{2+}–Cl^- models developed by DFT calculations. (b) Fourier transforms of the EXAFS plots in (a) revealing three main peaks corresponding to nearest neighbor interactions of the absorber (U) atom. (O_{ax} = axial oxygen atoms; O_{eq} = equatorial oxygen atoms)

• • •

Three main peaks are observable in the Fourier transform data (Fig. 5b), which arise due to single-scattering paths. The experimental data were fitted to theoretical curves using structural models obtained by DFT calculations (Fig. 4). For a pure UO_2^{2+} aqueous solution ($[Cl^-]$ = 0 M), there is no contribution from the scattering path corresponding to U–Cl, and therefore contributions are only from the axial (U–O_{ax} in Fig. 5b) and equatorial oxygen (U–O_{eq} in Fig. 5b) atoms. As the chlorine concentration is increased, a shoulder begins to emerge (U–Cl in Fig. 5b) to the right of the peak corresponding to the equatorial oxygen (U–O_{eq} in Fig 5b). With increasing temperature, this shoulder becomes more prominent indicating a change in coordination configurations at elevated temperatures. At the highest concentration ($[Cl^-]$ = 6 M) and temperature (100 °C), the DFT model with three equatorial oxygen and two chlorine atoms gives the best fit, revealing the stabilization of $[UO_2Cl_2(H_2O)_3]^0$ under hydrothermal conditions. This differs significantly from the $[UO_2(H_2O)_5]^{2+}$ and $[UO_2Cl(H_2O)_4]^+$ configurations existing at ambient conditions. We have therefore obtained vital information regarding the chemistry of actinide aqueous solutions at hydrothermal conditions.

Summary

High-pressure X-ray diffraction measurements of U-Si accident-tolerant nuclear fuels have provided key insights into their mechanical strength and structural behavior. X-ray absorption spectroscopy measurements of aqueous uranyl solutions at hydrothermal conditions meanwhile have revealed U(VI) coordination with chloride ligands present in the solutions, leading to significant changes in chemistry at elevated pressures and temperatures. Due to the common presence of chloride ions in groundwater, this finding is directly relevant to nuclear waste disposal in geological repositories. Both studies have yielded important information about actinide behavior at different stages of the nuclear fuel cycle and the potential for extreme conditions to change actinide properties. Therefore, it is essential to understand chemistry, structure, and properties of actinide solid and aqueous phases at high pressures and temperatures.

Acknowledgments

This work is a collaborative effort with a number of researchers: Enrique R. Batista, Hakim Boukhalfa, Diwash Dhakal, Andrew Gaunt, Robert A. Mayanovic, Changyong Park, Robert C. Roback, Cheng-Jun Sun, Tashiema Ulrich, Gaoxue Wang, Josh T. White, Hongwu Xu, and Ping Yang, who initiated and/or contributed to the above studies. Financial support was provided by the U.S. Department of Energy through the Glenn T. Seaborg Institute for the postdoctoral fellowship to Dr. Baker, and the LANL/LDRD program (#20180007DR).

Further reading

1. *J.L. Baker, G. Wang, T. Ulrich, J.T. White, E.R. Batista, P. Yang, R.C. Roback, C. Park, H. Xu, "High-pressure structural behavior and elastic properties of U_3Si_5: A combined synchrotron XRD and DFT study," J. Nucl. Mater., 2020, 520, 152373.*
2. *D. Dhakal, R.A. Mayanovic, J.L. Baker, H. Boukhalfa, H. Xu, C-J. Sun, "Design of a containment apparatus for synchrotron XAS measurements of radioactive fluid samples under high temperatures and pressures," Rev. Sci. Instrum., 2019, 90, 083108.*
3. *X. Guo, X. Lü, J.T. White, C.J. Benmore, A.T. Nelson, R.C. Roback, H. Xu, "Bulk moduli and high pressure crystal structure of U_3Si_2," J. Nucl. Mater., 2019, 523 135.*
4. *A. Timofeev, A.A. Migdisov, A.E. Williams-Jones, R. Roback, A.T. Nelson, H. Xu, "Uranium transport in acidic brines under reducing conditions," Nat. Commun., 2018, 9, 1469.*
5. *J.T. White, A.T. Nelson, D.D. Byler, D.J. Safarik, J.T. Dunwoody, K.J. McClellan, "Thermophysical properties of U_3Si_5 to 1773 K," J. Nucl. Mater., 2015, 456, 442.*
6. *S. Yagoubi, S. Heathman, A. Svane, G. Vaitheeswaran, P. Heines, J.-C. Griveau, T.L. Bihan, M. Idiri, F. Wastin, R. Caciuffo, "High pressure studies on uranium and thorium silicide compounds: Experiment and theory," J. Alloys Compd., 2013, 546, 63.*

Laurel Winter

Laurel Winter was a Seaborg Fellow from June 2015–May 2017 working under the mentorship of Ross McDonald, Neil Harrison, and Paul Tobash. Her research interests include understanding the electronic properties of correlated electron materials under the extreme of high magnetic fields. She is currently a staff member and the User Program Director of the National High Magnetic Field Laboratory-Pulsed Field Facility in the Materials Physics and Applications Division.

Probing the "Hidden Order" in URu_2Si_2

Laurel Winter
Los Alamos National Laboratory, Los Alamos, New Mexico

Understanding the behavior of actinide materials is important for issues such as developing new technology and predicting the aging of our nation's nuclear stockpile. These compounds have not been well studied and pose an additional challenge as they can display highly unusual behavior that deviates from patterns observed with elements from the rest of the periodic table. These anomalies can be traced to the nature of the 5f valence electrons, whose unique orbital shapes lead to electronic properties that vary between localized and itinerant behavior.

The alloy uranium ruthenium silicide (URu_2Si_2) displays a peculiar hidden order state, which has resisted explanation despite decades of experimental work. We sought to understand this state by applying large electric fields, an approach which has been useful for understanding other strongly-correlated materials. This method has been enabled by advances in modern device fabrication techniques, such as focused ion beam (FIB) lithography, which has made it possible to apply larger electric fields to a metal than previously achievable. By shedding light on the nature of this hidden order we expect to expand our understanding of 5f electron behavior and show that advances in modern device fabrication can lead to new experimental approaches that would otherwise not be possible.

Electron correlation

The behavior of "simple" metals can be accurately described by one-electron models, in which each electron can be considered as existing in a "sea" representing the averaged motion of other electrons. This is not the case for many d- or f-electron-containing materials for which these simple models fail due to the correlated nature of the electrons, i.e., each electron has a direct influence on its neighboring electrons. They are called correlated electron materials or strongly-correlated materials when the properties of a material deviate significantly from the simple one-electron model. Although it is a challenge to model these correlated electron materials in general, it is particularly difficult in 5f electron-containing materials where electrons can behave both as localized or delocalized (itinerant) particles, or often somewhere in between. This in-between 5f behavior often gives rise to exotic properties—superconductivity, magnetism, heavy-fermion behavior—in some actinide-containing materials.

One method to probe the electronic properties of materials is to subject them to an external environment and measure their response. In particular, extreme environments (such as low or high temperature, high pressure, and strong magnetic fields) can help reveal the properties of a material in a regime where only one external parameter is influencing its behavior. For actinide and actinide-based materials, these extreme environments can also expand our knowledge for continued stockpile stewardship efforts.

One strongly-correlated electron material that has been studied in various extremes is the alloy uranium ruthenium silicide, URu_2Si_2. Since the mid-1980s, condensed matter scientists have been using every tool imaginable to define the

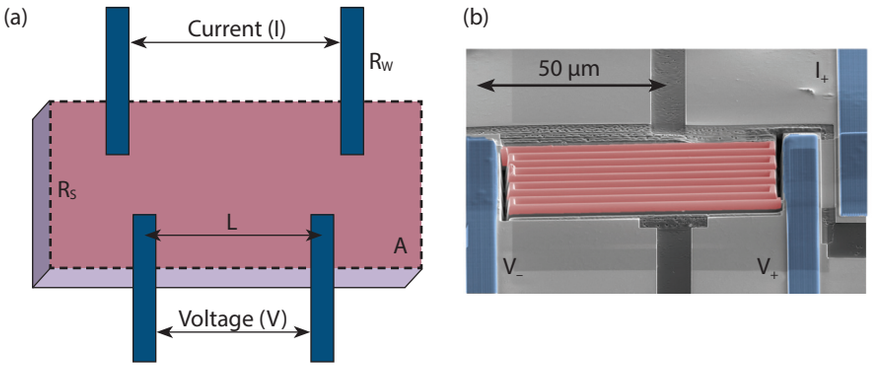

Figure 1. (a) Schematic of a sample with four wires attached for applying/measuring a current (I) and/or voltage (V). [L = distance between the voltage wires; A = cross-sectional area (red surface); R_s and R_w = resistance of sample and wires, respectively] (b) A color-enhanced electron-beam image of URu_2Si_2 sample, 5 µm thickness, milled by a focused ion beam (FIB). This process increased the length of the sample and increased the DC electric field produced in the sample while minimizing heating. The meander pattern is highlighted in red, while the voltage and current wires are highlighted in blue.

• • •

mysterious "hidden" order state of this system and determine what role the 5f electron behavior may be playing in the unknown state.

The hidden order phase

The earliest reports on URu_2Si_2 (1985/86) described a superconducting transition nominally at 1.5 K that varied with the sample quality, in addition to a 17.5 K transition that was insensitive to the sample quality, and was ascribed to a variety of magnetic orders. Further experiments disproved these magnetic order theories, as no evidence of long-range order below the transition temperature was found, i.e., the 17.5 K behavior is not due to a transition to a magnetic state or to a change in the structure of the material. Over time, the number of experimental probes applied to URu_2Si_2 has grown, however the results have led to more questions than answers regarding the nature of what has become known as the hidden order state, a name that highlights our inability to classify the condition of the material. One experimental approach that has not yet been brought to bear on this unknown state, and that has been pivotal in understanding other strongly-correlated states such as spin- and charge-density waves, is driving the conductivity of the hidden order state beyond the linear regime with the application of an electric field.

The heating problem

In order to effectively apply an electric field to URu_2Si_2, one inherent difficulty that had to be overcome is the side-effect of heating. This is due to both the fundamental properties of a metal and the method of producing the electric field. In order to apply an electric field to URu_2Si_2, an electric potential (voltage) is applied to the sample via small wires attached to the sample surface (Fig. 1). In the case of a prototypical metal (i.e., one that has a low resistance) the resistances of the wires attached to the sample are often significantly larger than the resistance of the sample itself, which means most of the voltage will be "lost" in the wires (and contacts) and not the sample. This then requires a significantly larger voltage to be applied to the wire/sample system in order to produce an electric field large enough to affect the electrons in the sample. Unfortunately, the current associated with such large voltages

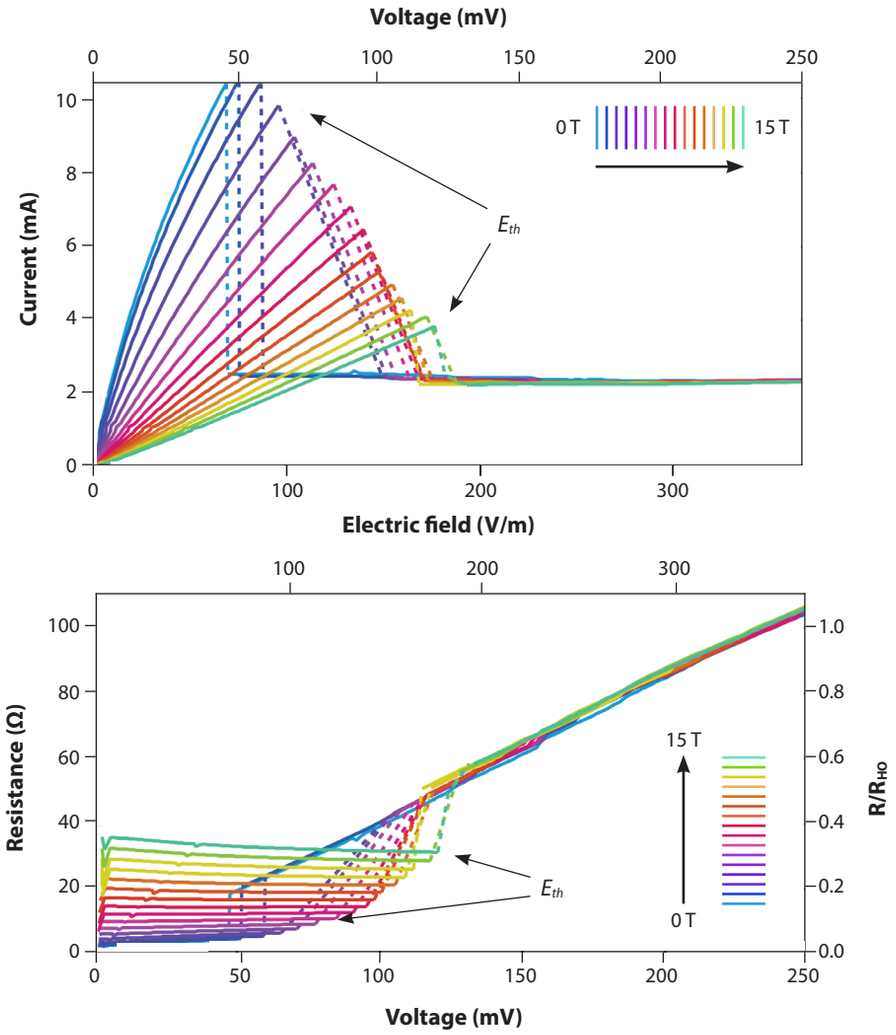

Figure 2. The current (*top*) and resistance (*bottom*) measured in a URu_2Si_2 sample as a function of electric field and voltage at different constant magnetic fields between 0 and 15 T at a temperature of 1.8 K in ^{4}He superfluid. The data show a sudden decrease in current (increase in resistance) that occurs at a critical threshold electric field (E_{th}) that increases with magnetic field strength. The strong linear behavior before E_{th} is indicative of minimal or no heating. In the bottom figure, the right axis corresponds to the ratio of the measured resistance to the resistance value at the hidden order transition in this sample (R/R_{HO}).

• • •

can inadvertently induce heating of both the wires and sample. This changes the experiment from one in which the material's properties are measured as a function of an applied electric field at constant temperature, to one in which the temperature is also changing, therefore introducing two variables whose effects on the sample cannot be completely separated. Since URu_2Si_2 must be cooled below 17.5 K to access the hidden order state, heating compromises the ability to perform such measurements.

Cooling down the electric field effects using lithography

There are limits to the amount of voltage that can be applied to a particular metal without causing heating via induced currents. These limits can only be altered in a situation in which the resistance of the material can be changed relative to that of the contacts. Fortunately, the resistance of a material can be changed readily, since it is related to the resistivity of a material and a geometrical factor (Fig. 1a). Therefore, the resistance of the sample can be increased by reducing the cross-sectional area and/or increasing the length. This means that a larger voltage (electric field) can be applied to the sample while reducing the amount of heating.

Both of these geometric changes can be made using focused ion beam lithography, which uses a beam of ions to cut or mill a material on a micron-scale (1×10^{-6} m). Using FIB lithography to "microstructure" URu_2Si_2 led to a hundred-fold increase in resistance, which was large enough for the sample resistance to dominate over that of the wires. Additionally, the meandering pattern created using lithography to increase the length of the sample (Fig. 1b) creates more contact between the sample and the cooling environment (helium gas or liquid), which aids in reducing the sample heating.

Unexpected resistance of URu_2Si_2

The effect of applying a large electric field to the hidden order state of URu_2Si_2 was studied in two regimes. In one regime, the sample was cooled to a temperature of 1.8 K in superfluid ^{4}He upon which a monotonically increasing electric field (via a voltage) was applied. We repeated the increases in applied electric field for constant magnetic fields between 0 and 15 T (Fig. 2). In the second regime, no magnetic field was applied. Instead, the monotonically increasing electric field was applied to the sample while a constant temperature above 1.8 K was maintained. This was repeated for temperatures between 2.6 and 20 K (Fig. 3). Our main observation in both regimes is an abrupt increase in resistance (corresponding to a drop in current) at a critical electric field (E_{th}). These measurements were repeated on two additional samples. They all showed qualitatively similar electric field-driven behavior despite differences in the sample geometries and sample purity.

Although we significantly reduced the likelihood of heating from the wires attached to the sample, we looked for evidence of heat driving the resistance behavior at E_{th}. Specifically, we calculated the ratio of the resistance measured during the voltage sweep to the resistance at the hidden order transition (R/R_{HO}, Fig 2b). If heating was the sole cause of the jump at E_{th}, such that it corresponded to heating the entire sample through the hidden order transition, then the jump in resistance would appear at $R/R_{HO} = 1$, which is about twice the value observed.

The linear (ohmic) behavior observed (Fig. 2) extends to higher electric fields and to a higher maximum current compared to that observed in the gas measurements (Fig. 3). This is due in part to the immersion of the sample in superfluid ^{4}He at 1.8 K, a liquid with a large heat capacity. In other words, it takes a large amount of energy to change its temperature. Since the temperature dependence studied in the second regime (described above) makes use of ^{4}He gas, which has less heat capacity than the superfluid state, heating effects become more evident, which are observed as the increase in curvature in the low electric field region (Fig. 3a).

From our gas measurements, there are two noteworthy observations. The first is that resistance decreases at an electric field that moves to lower values with increasing temperature (dotted line in Fig. 3b). This behavior is attributed to the suppression

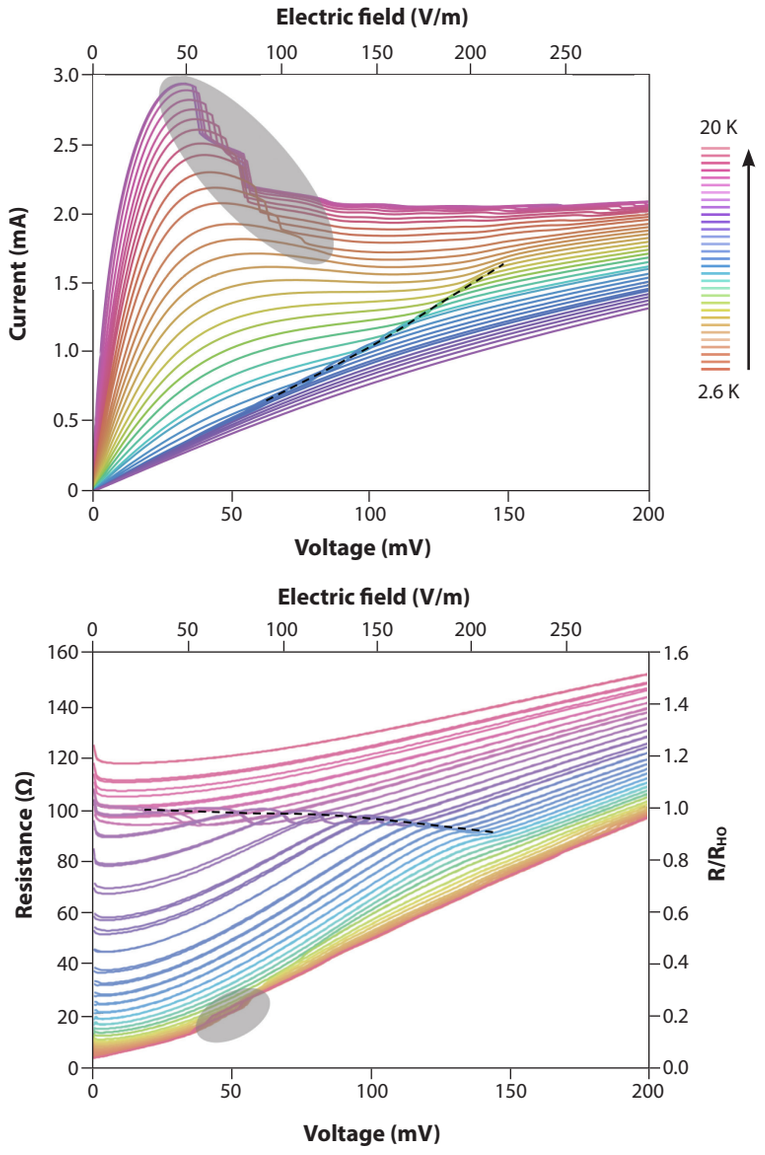

Figure 3. The current (*top*) and resistance (*bottom*) measured in the URu_2Si_2 sample as a function of electric field and voltage for different sample temperatures between 2.6 K and 20 K in ^{4}He gas. The right axis of the bottom figure corresponds to the ratio of the measured resistance to the resistance value at the hidden order transition in this sample (R/R_{HO}). The data show two regions of interest: (i) the shaded region which highlights a decrease in current (increase in resistance) at a critical threshold that increases with increasing temperature and (ii) the dotted line feature which corresponds to the thermal suppression of hidden order due to joule heating.

• • •

of the hidden order due to heating, which is supported by the disappearance of this behavior above 17.5 K and the repeated occurrence of this resistance drop around R_{HO} ~ 100 Ω. The second observation is a region in the data showing an increase in resistance at Eth that is minimally temperature dependent up to roughly 10 K (Fig. 3). Although smaller in amplitude, due to more heating, the resistance increase in this region is in agreement with the 1.8 K results. Since the resistance is once again less than R_{HO} we know at least some of the sample is at a temperature below 17.5 K (i.e., in the hidden order regime).

What does it all mean?

An increase in resistance at a given applied electric field (voltage) is rare in single crystal materials, like URu_2Si_2, and is typically only observed in carefully manufactured superlattice structures or certain semiconductors. One exception is in one-dimensional superconductors, in which an increase in resistance is observed at E_{th} due to the occurrence of a phase slip, whereby a very small amount of material goes "normal" (non-superconducting) and therefore a resistance is observed. This phase slip behavior can only occur in a quantum state of matter, such as superconductivity, in which the mathematical description (wavefunction) of the state has a phase and an amplitude at a minimum. Could this explain what we have observed? Unfortunately, such a description raises at least as many questions as it answers. For instance, if the hidden order state can be described mathematically in terms similar to that of a superconductor, why does it not exhibit the expected low voltage behavior of a superconductor?

Another less exciting possibility is that all of this can be explained by more complex inhomogeneous heating. Even though we trivially rule out homogenous heating through the hidden order transition, it is significantly more difficult to completely eliminate the possibility that very high thermal gradients are established in our sample.

Summary

Like the many previous studies of URu_2Si_2, these experiments have not conclusively unveiled the 40 year old mystery of its hidden order—more experiments are necessary to understand what is causing this non-linear behavior. To explore the significant and exciting possibility that these hidden order properties require a wavefunction description (i.e., a phase and an amplitude to describe it), further phase coherence studies, like Aharonov-Bohm experiments, typically performed on superconductors could be envisaged. The application of modern device fabrication techniques, such as FIB, is only the first step in understanding the truly quantum nature of many materials.

Acknowledgments

Internal collaborators: Ross McDonald, Neil Harrison, Eric Bauer (sample grower). External: Philip Moll (Ecole Polytechnique Federale de Lausanne Institute of Materials, Lausanne, Switzerland) who "microstructured" the samples, Brad Ramshaw (Cornell University, Ithaca, NY) and Arkady Shekhter (NHMFL, Tallahassee, FL). Funding was provided in part by the Department of Energy through the Los Alamos National Laboratory LDRD Program and the G.T. Seaborg Institute. The work was performed at the National High Magnetic Field Laboratory Pulse Field Facility, which is supported by the National Science Foundation Cooperative Agreement No. DMR-11557490, the State of Florida, and the US DOE.

Further reading

1. *N. Harrison, P.J.W. Moll, S.E. Sebastian, L. Balicas, M.M. Altarawneh, J.-X. Zhu, P.H. Tobash, F. Ronning, E.D. Bauer, B. Batlogg, "Magnetic field-tuned localization of the 5f –electrons in URu_2Si_2," Phys. Rev. B., 2013, 88, 241108(R).*
2. *N.P. Butch, J.R. Jeffries, S. Chi, J.B. Leão, J.W. Lynn, M.B. Maple, "Antiferromagnetic critical pressure in URu_2Si_2 under hydrostatic conditions," Phys. Rev. B., 2010, 82, 060408(R).*
3. *J.A. Mydosh, P.M. Oppeneer, "Colloquium: Hidden order, superconductivity, and magnetism: The unsolved case of URu_2Si_2," Rev. Mod. Phys., 2011, 83, 1301.*
4. *J.A. Mydosh, P.M. Oppeneer, "Hidden order behavior in URu_2Si_2 (A critical review of the status of the hidden order in 2014)," Phil. Mag., 2014, 94, 3642.*

Noah Jemison

Noah Jemison was a Seaborg Fellow from February 2019–March 2020 working under the mentorship of Hakim Boukhalfa and Ning Xu. His research interests include how redox-active contaminants, especially uranium, behave in the environment, and determining what processes are affecting the remediation of these contaminants by measuring isotope ratios. He currently works as a geochemist at Zeigler Geologic Consulting in Albuquerque, New Mexico where he works to develop better ways to apply geochemistry and geology to real-world issues, such as drought and groundwater contamination in rural communities.

Rapid Measurements of Actinide Isotope Ratios in Nuclear Materials

Noah Jemison
Zeigler Geologic Consulting, 13170 Central Ave SE, Suite B #137, Albuquerque, New Mexico

In order to properly characterize nuclear waste and perform nuclear forensics, we use an array of chemical tools. One critical tool is isotope ratio determination, in which uranium (U) and plutonium (Pu) isotopes are measured and compared to known nuclear materials. Actinide isotope ratios (such as the ratios of 234, 235 and 236 to 238 for uranium and 240 and 242 to 239 for plutonium) can provide evidence for the source and enrichment of nuclear materials. While U and Pu isotopes are radioactive, the isotopes listed above decay relatively slowly with half-lives in the thousands to billions of years. The slow decay of these isotopes allows us to treat these isotope ratios as effectively stable (under short timescales) whereas measuring short-lived isotopes, such as ^{238}Pu and ^{241}Pu, can provide information on radioactive decay of nuclear material.

Uranium and plutonium isotope ratios are typically measured on a thermal ionization mass spectrometer (TIMS). This involves loading a sample onto a filament and heating it to release and ionize the actinides. As actinides are released, a magnet separates different isotope masses. These isotope masses are simultaneously measured in detectors to determine the amount of each isotope in a sample. However, this method is time consuming due to the filament loading and heating process. Each analysis (excluding sample loading time) takes approximately 40 minutes per sample. For rapid isotope analysis, there are a number of simpler methods available.

An example of an alternative, quicker method for detecting actinide isotopes is high-resolution inductively coupled plasma mass spectrometry (HR-ICP-MS). This instrument uses a magnet to separate isotope masses similar to a TIMS, but HR-ICP-MS also has several key differences. The HR-ICP mass spectrometer scans through different isotope masses rapidly, instead of setting the magnet to a certain mass as conducted with a TIMS. The high resolution method only detects a single isotope at a time, which makes measurements less precise than TIMS. Samples are introduced into the HR-ICP-MS typically as liquid solutions and do not require being loaded onto filaments or heating those filaments, which speeds up sample processing. By measuring actinide isotope ratios on an HR-ICP-MS, we can rapidly analyze samples that do not require high precision. This method allows us to characterize nuclear waste and perform nuclear forensics more quickly.

We analyzed three uranium isotope standards and two plutonium metals with known isotope ratios. During subsequent analysis, we compared our isotope ratio measurements to these known isotope values to determine precision and accuracy of our methods. Analyzing ^{234}U/^{238}U, ^{235}U/^{238}U, and ^{236}U/^{238}U in uranium materials or ^{240}Pu/^{239}Pu and ^{242}Pu/^{239}Pu in plutonium materials required only five minutes per sample. This sample time includes a wash cycle, sample introduction, and analysis. Using this technique, we can analyze approximately eight samples in the time it takes to measure one sample on a TIMS instrument.

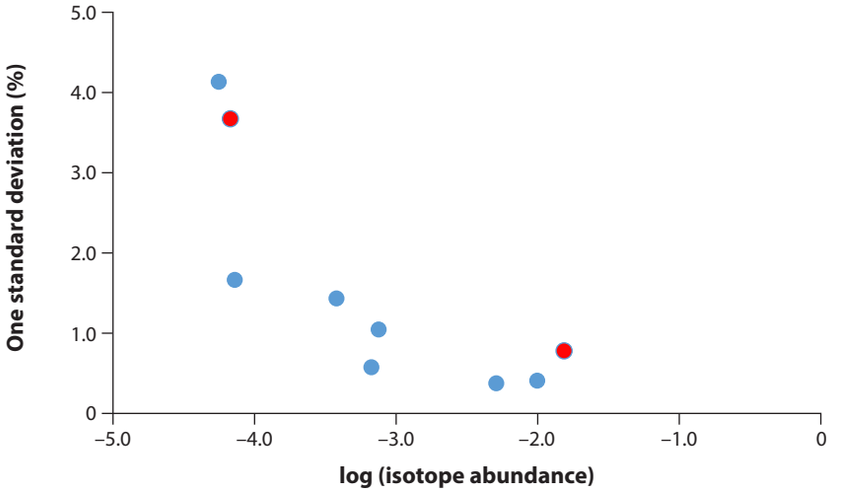

Figure 1. Uncertainty of isotope ratios. Logarithmic-scale plot of analytical uncertainty (one standard deviation) versus isotope abundance. With miniscule isotope abundances, such as ^{242}Pu, measurement uncertainty of ^{242}Pu/^{239}Pu is high and precision is low. With higher levels of isotopes, such as ^{235}U, greater precision is achieved such as for ^{235}U/^{238}U.

Precision and accuracy

Although precision and accuracy sound like synonyms, the terms have slightly different meanings. Precision corresponds to how close all measurements are to each other. Accuracy, meanwhile, corresponds to how close measurements are to a specific reference value. We sacrifice some precision using HR-ICP-MS versus the high-precision TIMS. Depending on the isotope abundance (the percentage of each isotope), the uncertainty (one standard deviation) of our measurements ranges from 0.1% to 4.2%. The uncertainty of our measurements inversely correlates with the isotope abundances (Fig. 1). With increased detection of more abundant isotopes, one can better estimate these isotope ratios. Our measured uncertainty using HR-ICP-MS is five to ten times higher than that with TIMS. Accuracy remains high using the HR-ICP-MS. No systematic bias is detected, so measurements all clump around the known isotope values of the uranium isotope standards and plutonium metals.

Summary

Our measurements demonstrate that HR-ICP-MS provides a rapid alternative method to TIMS for measuring isotope ratios in nuclear materials. This method could allow for faster removal of nuclear waste, release of nuclear inventory, and shipment of nuclear material. In addition, similar isotope methods could be developed for other elements. Isotope ratios of americium and neptunium could provide greater nuclear forensic capabilities for example. Furthermore, ratios of non-actinides may also be useful data in nuclear forensics. The lower precision of HR-ICP-MS limits applications since detection of small changes in isotope ratios (less than 1%) is very difficult or impossible. However, if sources of nuclear material have significantly different isotope ratios, these differences could be detected using HR-ICP-MS. This method may also be used for various other applications, such as detecting different sources of contaminants. By developing isotope ratio methods, we can decrease analysis time for numerous materials in order to rapidly source materials and detect certain chemical and nuclear reactions.

David Frazer

David Frazer was a Seaborg postdoc fellow from November 2018—June 2020 during which time he worked on powder processing, thermophysical characterization, and small scale testing of accident tolerant fuels. In addition to small scale mechanical testing, David has investigated heavy liquid metals as advanced coolants for nuclear and thermal solar systems and worked on advanced characterization of nuclear materials using electron microscopes and focused ion beam techniques. He is currently a Staff Scientist at Idaho National Laboratory where he is performing small scale mechanical testing on materials related to the nuclear industry. This includes advanced accident tolerant fuels, advanced cladding concepts and neutron irradiated materials.

Small-Scale Mechanical Testing of Actinide Compounds

David Frazer
Idaho National Laboratory, Idaho Falls, Idaho

Nuclear reactors produce 20% of the electrical power in the United States and represent a viable carbon-reducing energy source for future electrical production. Current reactors use uranium dioxide as fuel, which undergoes internal structural changes as it is used—mainly from radiation effects and the formation of fission products. For operational safety and modeling accident behavior, it is imperative to understand these changes in mechanical properties because failure of the fuel rod can lead to release of radioactive material. Furthermore, this understanding could lead to longer fuel lifetimes, improving the efficiency of reactors.

The core of a nuclear reactor contains Zircaloy fuel rods filled with uranium dioxide (UO_2) which produce heat and, consequently, electricity via steam turbines. The zirconium cladding is used as the first barrier to prevent radioactive material release. As the fission reactions proceed, solid and gaseous fission products, heat, and neutrons are produced in the fuel pellets. The solid and gaseous fission products cause the pellets to swell—the incipient gas atoms coalesce into bubbles in the fuel and the solid products form precipitates that occupy more space. Furthermore, the cladding slowly creeps down to the UO_2 pellet due to the high pressure of the coolant. The swelling of pellets and the decreasing diameter of the cladding rod from cladding creep cause the fuel and cladding to come into contact while in the reactor core. This causes both mechanical and chemical pellet-clad interactions (PCMIs and PCCIs, respectively) which can result in cladding failure and the subsequent release of radioactive material into the coolant.

Investigating the mechanical properties of the fuel and cladding material before, during, and after use is critical to understanding and modeling PCMIs. However, the high radiation levels emitted by spent nuclear fuel makes measuring mechanical properties challenging because it has to be performed in specialized safe containment boxes known as hot cells. The use of hot cells greatly increases the time and cost of post-irradiation examination. Additionally, spent nuclear fuel contains many microstructural zones and cracks making macroscale mechanical testing of the pellet difficult (Fig. 1). A fresh fuel pellet with a homogeneous microstructure can be measured using macroscale tests, such as compression, however it would be nearly impossible to obtain valid results by performing a similar test on spent fuel because of the irregular cracking and heterogeneous microstructure.

Small-scale mechanical testing

Small-scale mechanical testing (SSMT) is an approach that measures mechanical properties using small volumes of material. This allows measurements to be performed without hot cells, greatly reducing the cost and time of post-irradiation examination. This is especially important as it can shorten the timeline of qualifying new fuels for use in nuclear reactors. SSMT can measure the same properties as

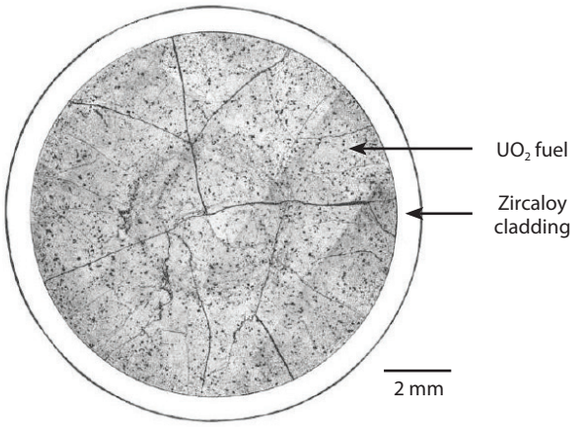

Figure 1. A fuel cross section at irradiation to 42 kW/m. The large amount of cracking in fuel can be observed.

• • •

macroscale techniques with smaller sample volumes and allows different microstructural features in the material to be targeted. SSMT includes techniques based on nanoindentation and focused ion beam (FIB) methodology, including microcompression, micro-bending, and micro-tensile procedures. Nanoindentation and FIB-based techniques were first developed in the 1980s and early 2000s, respectively, and have found increased use in the nuclear materials community over the last decade.

Nonetheless, there are some challenges with implementing SSMT techniques with nuclear materials due to the small size of the testing specimens (5–30 micrometers). Because a small volume of material is sampled in these tests, the mechanical properties of individual grains can skew the measurements. Grain orientation perpendicular or parallel to applied stress will produce different values for the same property due to asymmetry within the crystal structure (Fig. 2). Due to the chemical bonds between the uranium and oxygen ions in UO_2, this material has different mechanical properties in different orientations in the solid state. This is borne out clearly in measurements—the elastic modulus in the [100] direction is 333 GPa, while in the [111] direction it is 163 GPa (these directions are given in Miller indices, a vector representation for the orientation of a crystal lattice plane, defined as the reciprocals of the fractional intercepts which the plane makes with the crystallographic axes). During macroscale testing, a sample large enough to contain many grains in the cross-section is used so the average value is measured.

In order to reduce these errors caused by sample anisotropy, there are two solutions which can be employed. One is to perform enough individual measurements to get a statistical average of the mechanical properties. The second is to have prior knowledge of the microstructure and grain orientation before SSMT. The first solution is useful for techniques like nanoindentation in which tens-to-hundreds of indents can be performed an hour, allowing us to obtain the statistical average of the mechanical properties. The second solution provides the additional benefit of evaluating the microstructure after irradiation which can help us understand PCMIs, PCCIs, and other phenomenon occurring in the fuel and cladding.

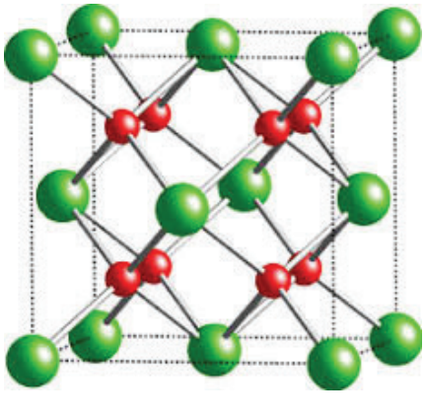

Figure 2. The crystal structure of UO_2. The crystal structure of material describes how the atoms are arranged—in an individual grain, all of the atoms are ordered in the same direction as dictated by the crystal packing shown here. [green = uranium; red = oxygen]

• • •

Despite the challenges, SSMT shows much potential to provide insight and accelerate nuclear materials development. Micro-tensile testing has been used to evaluate the reduction in elongation plasticity from irradiation exposure. Additionally, due to the low cost, ion beams have been used to expedite fuel material evaluation for nuclear reactors. However, because the ions are charged particles they only penetrate surface depths of the order of tens of micrometers. This limited penetration means that the technique is not useful in macroscale testing, however it can be used with smaller samples using SSMT techniques. Measuring small volumes of material also allows for measuring of new advanced fuel forms at the laboratory scale to evaluate how different processing routes affect mechanical properties. Furthermore, modern nanoindentation instruments have the ability to measure samples at off-ambient conditions to evaluate the mechanical properties over a temperature range including operational temperature.

Instrumentation

Indentation is perhaps the most commonly applied means of testing the mechanical properties of materials. A nanoindentation instrument can measure a variety of these properties depending on the tip and loading scheme used. The most common properties measured with a nanoindenter are the hardness (resistance to localized plastic or permanent deformation) and elastic modulus (resistance to elastic or non-permanent deformation) over temperature.

The instrument used for these studies was a Hysitron Triboindenter (Fig. 3b). It includes two loading heads with different ranges and can perform experiments up to 800°C. A challenge with performing high temperature nanoindentation experiments comes from the unwanted oxidation of uranium-based materials. Therefore, additional feedthroughs were installed to supply the test chamber with a reducing or inert gas in order to create a stable testing environment.

Nanoindentation is instrumented, meaning that the depth and load are continuously monitored to give datasets which can be plotted as load-unloading curves (Fig. 3a). These curves are then used to measure the reduced modulus which can be used to calculate the elastic modulus and the hardness of the material (Fig. 4).

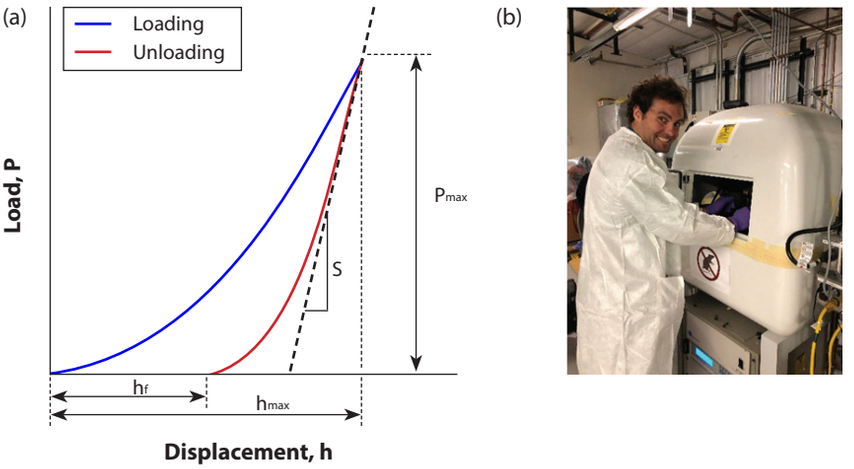

Figure 3. (a) A representative load-unloading curve from a nanoindentation experiment. The initial slope of the unloading curve is used to measure the reduced modulus which allows for calculating the elastic modulus. (b) The author using the instrument at LANL.

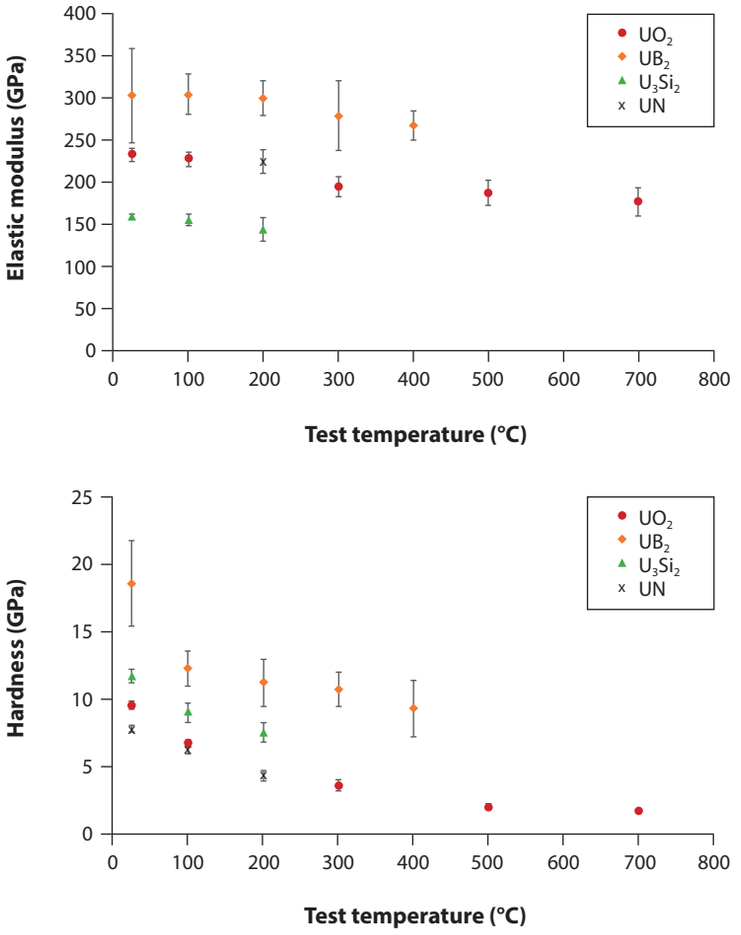

Figure 4. The elastic modulus (*top*) and hardness values (*bottom*) of the UO_2 and advanced accident-tolerant nuclear fuel candidates UB_2, U_3Si_2, and UN versus the temperature tested with the nanoindentation system.

Current nuclear fuels

The fuel currently used in most operating nuclear reactors is UO_2. For a better understanding of the PCMIs occurring in reactors today we need a more detailed knowledge of the mechanical properties of spent fuel, and in order to apply these SSMT techniques to spent fuel, they first need to be proven on fresh fuel. At Los Alamos National Laboratory (LANL), the mechanical properties of UO_2 were measured using nanoindentation at temperatures from ambient to 700°C. It was observed that the elastic modulus decreases in a linear manner and the hardness in an exponential manner, as would be expected in this temperature range (Fig. 4). The values of elastic modulus agree well with other elastic modulus values collected using other techniques on a macroscale. This agreement suggests that nanoindentation can be used as effectively as macroscale techniques to measure changes in the mechanical properties of UO_2 after use in a nuclear reactor.

Advanced accident-tolerant nuclear fuels

The 2011 Fukushima Daiichi nuclear accident has prompted several countries to evaluate advanced accident-tolerant fuels. In particular, fuels with higher thermal conductivity and uranium density are being investigated. A variety of different fuel forms have been proposed such as U_3Si_2, UN, and UB_2. Using elevated temperature nanoindentation we can rapidly obtain mechanical property data that can be used understand potential PCMIs of these accident-tolerant fuel forms. It was observed that the elastic moduli of these materials decrease in a linear manner and the hardness in an exponential manner (Fig. 4). Prompt mechanical testing data allows for faster iterations when developing new materials, which could potentially increase the speed of developing new fuels and materials for the nuclear industry.

Summary

Small-scale mechanical testing has the ability to measure the mechanical properties of a wide range of materials of interest to the nuclear materials community using small sample volumes. The development of these techniques for use with fresh fuels, as demonstrated here, has the potential to reduce the cost and time of post-irradiation examination. Additionally, new data acquired through these studies could improve the modeling of pellet-clad mechanical interactions during operation of a nuclear reactor. Finally, these savings could greatly shorten the timeline for developing and employing new accident-tolerant fuels and structural materials for future nuclear reactor systems.

Further reading:

1. *C.T. Walker, "Electron probe microanalysis of irradiated nuclear fuel: an overview" J. Anal. At. Spectrom. 1999, 14 447.*
2. *W. Zhou, W. Zhou, "Enhanced thermal conductivity accident tolerant fuels for improved reactor safety—A comprehensive review," Ann. Nucl. Energy, 2018, 119, 66–86.*
3. *P. Hosemann, "Small-scale mechanical testing on nuclear materials: bridging the experimental length-scale gap," Scr. Mater., 2018, 143, 161–168.*
4. *W.C. Oliver, G.M. Pharr, "An improved technique for determining hardness and elastic modulus using load and displacement sensing indentation experiments," J. Mater. Res., 1992, 7, 1564–1583.*
5. *J.M. Wheeler, D.E.J. Armstrong, W. Heinz, R. Schwaiger, "High temperature nanoindentation: The state of the art and future challenges," Curr. Opin. Solid State Mater. Sci., 2015, 19, 354–366.*

Searching for Topological Phases in Lanthanide and Actinide Compounds

Nicholas Sirica
Los Alamos National Laboratory, Los Alamos, New Mexico

Ordered states of matter have traditionally been categorized by their broken symmetries, such as the loss of symmetry when spins order in a ferromagnet or liquid freezes into a crystalline solid. Nonetheless, over the past decade a new way of classifying matter has captivated scientists, in which materials can be distinguished by the geometric characteristics, or topology, of their electronic states. These topological materials, which include topological insulators in addition to Dirac and Weyl semimetals, hold great promise for future use in quantum information science and electronics. They possess electronic states that are protected from back scattering, and have potential use as topological switches akin to electronic transistors.

Marrying topology with strong electron interactions, such as those found in lanthanide and actinide based compounds, offers a route to control topological properties by exploiting the strongly coupled electron, lattice, and spin degrees of freedom present in these materials. Theoretical calculations have predicted the presence of topological properties in both Kondo insulators and actinide-based Mott insulators. To date, however, such predictions have proven difficult to unambiguously verify experimentally, due to the characteristically small energy scales (< 10 meV) found in these systems.

To address this problem, we focused on the role that nonlinear optical techniques have in elucidating non-trivial topology. Central to this study is the measurement of helicity-dependent photocurrents (i.e., light-induced currents that depend on the degree of circular polarization) probed in a contact-free manner using terahertz (THz) emission spectroscopy. Previous claims in the literature suggest photocurrent generation to be intrinsic to such physical properties as spin-momentum locking and Weyl fermion chirality in Weyl semimetals.

Tantalum arsenide

Beginning with a prototypical example of a Weyl semimetal, tantalum arsenide (TaAs), we observed robust helicity-dependent, ultrafast photocurrents, exhibiting the same fundamental behavior as found in static experiments (Fig. 1). However, a detailed consideration of crystal symmetry revealed that such photocurrents do not provide a measure of non-trivial topology in these materials.

Such findings have important implications for Kondo-Weyl semimetals, in which the small energy scales involved make photocurrent generation a promising route for determining topology experimentally. Thus, unless crystal mirror symmetries are lifted to allow for the generation of quantized photocurrents specific to Weyl fermion excitation, the mere presence of helicity-dependent photocurrents in candidate Kondo-Weyl semimetals has no bearing on their topological properties.

Nicholas Sirica

Nicholas Sirica graduated with a BS in physics and chemistry from Bridgewater College in 2010. He went on to pursue a PhD in experimental condensed matter physics from the University of Tennessee, where he worked in the strongly correlated electron spectroscopy group lead by Prof. Norman Mannella. He joined Los Alamos National Laboratory as a Seaborg Fellow in 2017, where his postdoctoral studies focused on nonlinear optical spectroscopy of topological semimetals with Dr. Rohit Prasankumar and Dr. Dmitry Yarotski. He is now a Scientist (MPA-CINT) in the laboratory for ultrafast material and optical science.

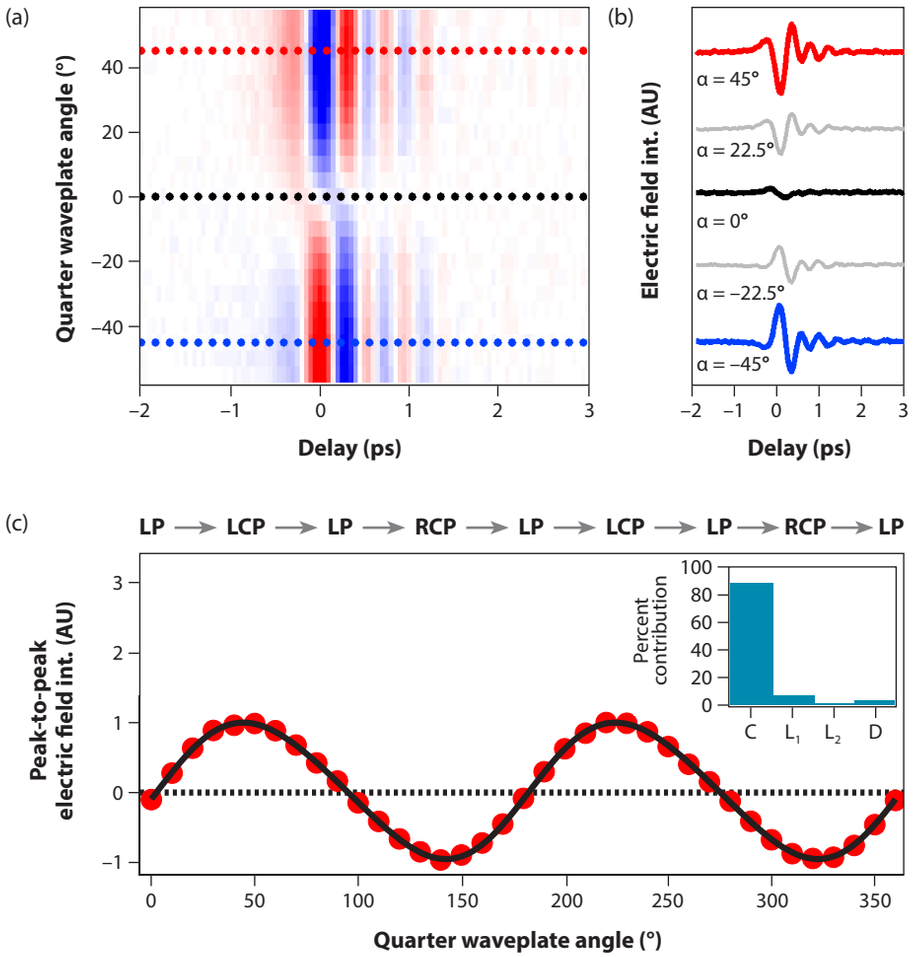

Figure 1. (a) False color plot and (b) select time-dependent THz traces, illustrating the polarity reversal of the emitted THz waveform upon changing the helicity of the optical generation pulse. Traces shown in (b) are obtained using quarter waveplate (QWP) angles of +/–45, +/–22.5, and 0°, corresponding to right/left circular, elliptical or linear polarizations, respectively. (c) Peak-to-peak electric-field amplitude plotted as a function of QWP angle and fit [LP = linear polarization; LCP/RCP = left/right circular polarization]. The inset illustrates the relative weight of each fitting component [C = circular photgalvanic; L_1, L_2 = linear photogalvanic; D = polarization independent offset].

• • •

In addition to ultrafast, helicity-dependent photocurrents, polarization-independent photocurrents were found along the non-centrosymmetric c-axis of TaAs. Due to the presence of a polar Ta–As bond lying along this axis, we were able to attribute such a photocurrent to a shift in electron charge density following photoexcitation. This so-called shift current is believed to underlie both the colossal bulk photovoltaic effect and the giant nonlinear response seen in second harmonic generation (SHG). Therefore, in an effort to probe the dynamics intrinsic to such a shift in charge density, we performed time-resolved SHG experiments on TaAs. A clear signature was found for a current-induced symmetry broken state that emerges following photoexcitation (Fig. 2).

A critical aspect regarding the nature of this photoinduced state relies on the relative contribution that crystalline and electronic structures have in driving the transient symmetry change. To address this question, we performed time-resolved

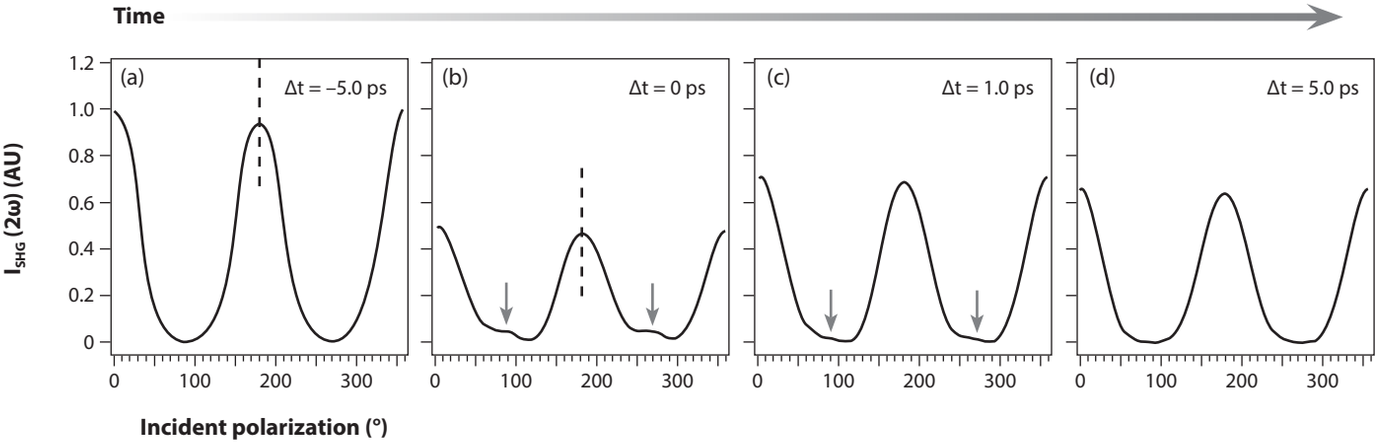

Figure 2. Snapshots of the second harmonic generation (SHG) pattern (2ω ~ 3.1 eV) measured along the [1,1,-1] axes (a–d) for various pump delays: (a) Δt = –5.0 ps, (b) 0 ps, (c) 1.0 ps and (d) 5.0 ps. Arrows in (b) and (c) denote the presence of transient, asymmetric lobes in the photoexcited state, while a small 2.5° rotation of the SHG pattern along [1,1-1] is evident from the dashed line in (b).

• • •

X-ray diffraction experiment using the Linear Coherent Light Source (LCLS) at the Stanford Linear Accelerator (SLAC). These diffraction studies did not show any structural changes occurring on the same timescale as the emergent current-induced state, verifying that transient symmetry breaking in TaAs following photoexcitation is purely electronic in origin.

Considering that the ultrafast timescale of this photoinduced phase (< 1 ps) is equivalent to that deduced from THz emission for the shift current, we argue that our time-resolved SHG measurements directly probe the dynamics intrinsic to a shifted charge density in these materials.

Gaining new insight into the electron dynamics of heavy fermions

Heavy fermion materials are a type of intermetallic compound which contain 4f or 5f elements with unfilled valence bands. The name "heavy fermion" derives from the observation that the fermion (electron) behaves as if it has an effective mass greater than its rest mass, which can have unusual effects on material properties.

Momentum (k) integrated ultrafast optical measurements have shown the formation of a hybridization gap in heavy fermions to profoundly impact relaxation dynamics through setting up the condition for a Rothwarf-Taylor phonon bottleneck. A quantitative description of the dynamics often requires the use of a stretched exponential, suggesting there to be a distribution of relaxation times. This could be due to an anisotropy in the hybridization gap arising from a k-dependence.

We proposed to explore k-resolved electron relaxation dynamics directly by performing time- and angle-resolved photoemission spectroscopy. This approach has the advantage that any anisotropy in the hybridization gap can be studied, along with the intrinsic timescale associated with the dressing of a quasi-particle as it couples to one or more bosonic modes.

Definitions

Fermions	A class of spin-½ particles that includes the electron.
Weyl fermions	Spin-½ particles with no mass, which carry charge and handedness.
Dirac fermions	Spin-½ particles with no mass, which carry charge but no handedness.
Topological insulators	Materials which are insulators in the bulk, but conduct very well on the surface. Topology here refers to the mathematical properties of the surface.
Weyl semimetals	Solid-state crystals whose low energy excitations are Weyl fermions even at room temperatures.
Kondo insulators	Also known as heavy fermion semiconductors, these are materials with strongly correlated electrons that open up a narrow band gap at low temperatures due to the strong-correlation phenomenon called the Kondo effect.
Mott insulators	Materials that should conduct electricity under conventional band theories, but are found to be insulators when measured. This due to electron-electron interactions.
Kondo-Weyl semimetals	A new type of quantum material proposed in 2017 which possesses Weyl fermions that are tied to both strong electron correlations and nontrivial topology, originating from the Kondo effect.

The Seaborg fellowship funded work to upgrade the experimental setup, allowing for such measurements to be performed. Several new parts were installed including a state-of-the-art, six degree-of-freedom sample manipulator, an electron-beam heater, a low energy electron diffractometer, and a new mu-metal chamber. Work on the angle-resolved photoemission spectroscopy (ARPES) chamber is nearly complete and photoelectrons are now being generated. Presently, work on the extreme ultraviolet, laser-based light source is underway so as to maximize photon flux at the high probe energies required for lanthanide and actinide based materials. Given our recent progress, we anticipate having a fully functioning time resolved-ARPES (tr-ARPES) system by the end of 2021.

Summary

The use of nonlinear optics as an extreme ultraviolet light source (tr-ARPES) or as a spectroscopy (THz emission and SHG) provides many new opportunities to study f-electron systems. We are developing these techniques by performing THz emission and time-resolved SHG spectroscopy on the prototypical Weyl semimetal TaAs, whose results have important implications for Kondo-Weyl semimetals. Furthermore, by developing a tr-ARPES light source specifically tailored to study f-electron materials, we will soon be able to shed new light on the interplay between local magnetic moments and itinerant conduction electrons in these material systems.

Acknowledgments

Support for this work was provided by the Seaborg Institute and Laboratory Directed Research and Development at Los Alamos National Laboratory.

Further reading:

1. *N. Sirica, R.I. Tobey, L.-X. Zhao, G.F. Chen, B. Xu, R. Yang, B. Shen, D.A. Yarotski, P. Bowlan, S.A. Trugman, J.-X. Zhu, Y.M. Dai, A.K. Azad, N. Ni, X.G. Qiu, A.J. Taylor, R.P. Prasankumar, "Tracking ultrafast photocurrents in the Weyl semimetal TaAs using THz emission spectroscopy," Phys. Rev. Lett., 2019, 122, 197401.*
2. *N. Sirica, P.P. Orth, M.S. Scheurer, Y.M. Dai, M.-C. Lee, P. Padmanabhan, L.T. Mix, S.W. Tietelbaum, M. Trigo, L.X. Zhao, G.F. Chen, B. Xu, R. Yang, C. Hu, B. Shen, C.-C. Lee, H. Lin, T.A. Cochran, S.A. Trugman, J.-X. Zhu, M.Z. Hasan, N. Ni, X.G. Qiu, A.J. Taylor, D.A. Yarotski, R.P. Prasankumar, "Photocurrent-driven transient symmetry breaking in the Weyl semimetal TaAs," submitted to Nat. Mater., 2020, arXiv2005.10308.*

Actinide Research Quarterly is published by Los Alamos National Laboratory and is a publication of the Glenn T. Seaborg Institute for Transactinium Science, a part of the National Security Education Center. ARQ (est. 1994) highlights research in actinide science in such areas as process chemistry, metallurgy, surface and separation sciences, atomic and molecular sciences, actinide ceramics and nuclear fuels, characterization, spectroscopy, analysis, and manufacturing technologies.

LA-UR 21-26079

Address correspondence to:
Actinide Research Quarterly
c/o Editor
Mail Stop T-001
Los Alamos National Laboratory
Los Alamos, NM 87545

ARQ can be read online at:
www.lanl.gov/arq

If you have questions, comments, suggestions, or contributions, please contact the ARQ staff at:
arq@lanl.gov

National Security Education Center
David L. Clark, Director

G. T. Seaborg Institute for Transactinium Science
Science Advisors
Franz Freibert, Director
Ping Yang, Deputy Director

Editor
Owen Summerscales

Designers/Illustrators
Don Montoya
Owen Summerscales

Actinide Research Quarterly
Mail Stop T001
Los Alamos National Laboratory
Los Alamos, NM 87545

arq@lanl.gov

Presorted Standard
U.S. Postage Paid
Albuquerque, NM
Permit No. 532

Los Alamos NATIONAL LABORATORY

THE GLENN T. SEABORG INSTITUTE

NNSA